

# Selection of dune shapes and velocities. Part 1: Dynamics of sand, wind and barchans.

Bruno Andreotti<sup>1</sup>, Philippe Claudin<sup>2</sup>, and Stéphane Douady<sup>1</sup>

<sup>1</sup> Laboratoire de Physique Statistique de l'Ecole Normale Supérieure, 24 rue Lhomond, 75231 Paris Cedex 05, France.

<sup>2</sup> Laboratoire des Milieux Désordonnés et Hétérogènes (UMR 7603), 4 place Jussieu - case 86, 75252 Paris Cedex 05, France.

October 30, 2018

**Abstract.** Almost fifty years of investigations of barchan dunes morphology and dynamics is reviewed, with emphasis on the physical understanding of these objects. The characteristics measured on the field (shape, size, velocity) and the physical problems they rise are presented. Then, we review the dynamical mechanisms explaining the formation and the propagation of dunes. In particular a complete and original approach of the sand transport over a flat sand bed is proposed and discussed. We conclude on open problems by outlining future research directions.

**PACS.** 45.70.-n Granular systems – 47.54.+r Pattern selection; pattern formation

## 1 Introduction

After pioneering works by Bagnolds [1], the investigation of dune morphology and dynamics has been the exclusiveness of geologists and geographers. For nearly four decades, they have been reporting field observations about the condition under which the different kinds of dunes appear as well as measuring their velocity [2,3,4,5,6], their shape [3,4,5,6,7,8,9,10,11,12], the patterns they form, the size distribution of sand grains, etc. More recently dunes have attracted the interest of physicists [12,13,14,15,16,17,18,19] motivated by the poetry of deserts or by the physics they conceal, by the dryness of saharan countries or by the observation of dunes on Mars.

The aim of this paper is to give an overview of this domain. It is conceived as a pedagogical review of field

observations and of the dynamical mechanisms important for dune morphogenesis, followed by a conclusion discussing some of the problems remaining open. It is followed by a second part devoted to the derivation of a simple model predicting the shape and velocity of two-dimensional dunes.

In this article, we will mainly focus on the barchan which is the simplest, and consequently the most studied form of sand dunes. A barchan is a crescentic dune as that shown on figure 1, propagating downwind on a firm soil [1,20]. When the direction of the wind is almost constant, these dunes can maintain a nearly invariant shape and size (3–10 m) for very long times (1–30 years) [1,3]. The basic dynamical mechanism explaining the dune propagation is

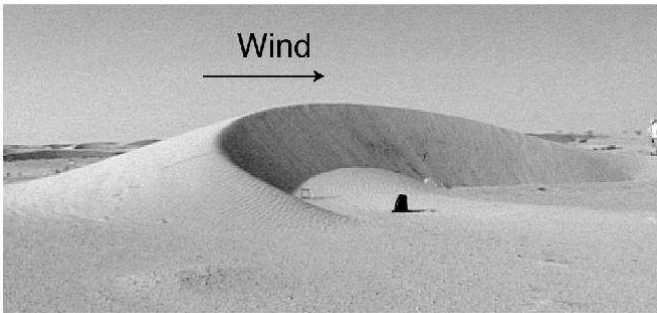


**Fig. 1.** The barchan is a dune with a characteristic crescent shape, possibly isolated. A small dune ( $\simeq 3$  m high) as that shown (Mauritania), propagates downwind at one hundred meters per year, typically.

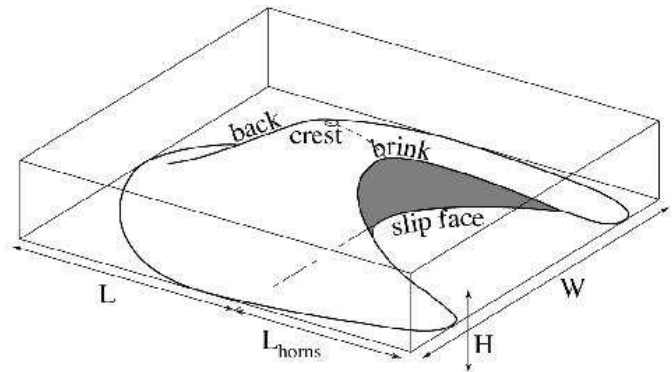


**Fig. 2.** Sketch of a barchan dune. In first approximation, the dune morphology can be described by four morphologic parameters: the length  $L$ , the width  $W$ , the height  $H$  and the horn length  $L_{horns}$ .

simple (see figure 2): the back of the dune is eroded by the wind; the sand transported in saltation is deposited at the brink, and is redistributed on the slip-face by avalanches. In this picture, a dune keeps the same amount of sand. In reality, the global mass evolution results from the balance between the sand supply at the back and the leak at the horns.

Starting from this overview of barchan properties, we give in section 2 a short review of the field observations, concerning in particular the morphology and velocity scaling laws. The dynamical mechanisms involved in erosion and sand transport are presented in section 3 and the corresponding dimensionless parameters as well as the scaling laws are discussed. Finally, in section 4, we sort the facts both validated by experimental measurements and explained by consistent theories from the problems remaining partly or totally open up to now.

## 2 Field observations

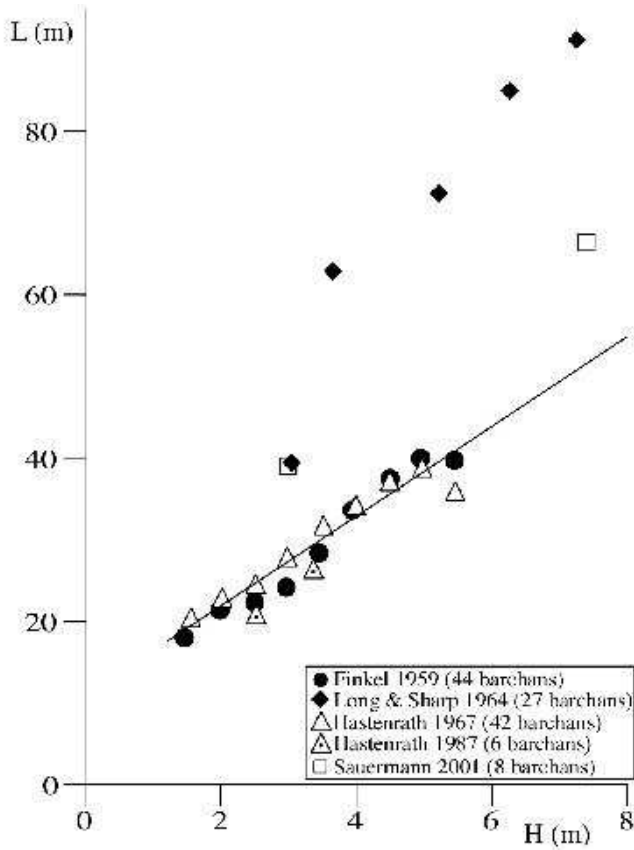


**Fig. 3.** Relationship between the dune length  $L$  and height  $H$  determined from field measurements averaged by ranges of heights. The solid line is the best linear fit to the points corresponding to barchans from the Arequipa region in Southern Peru (Finkel [3] and Hastenrath [6,9]).

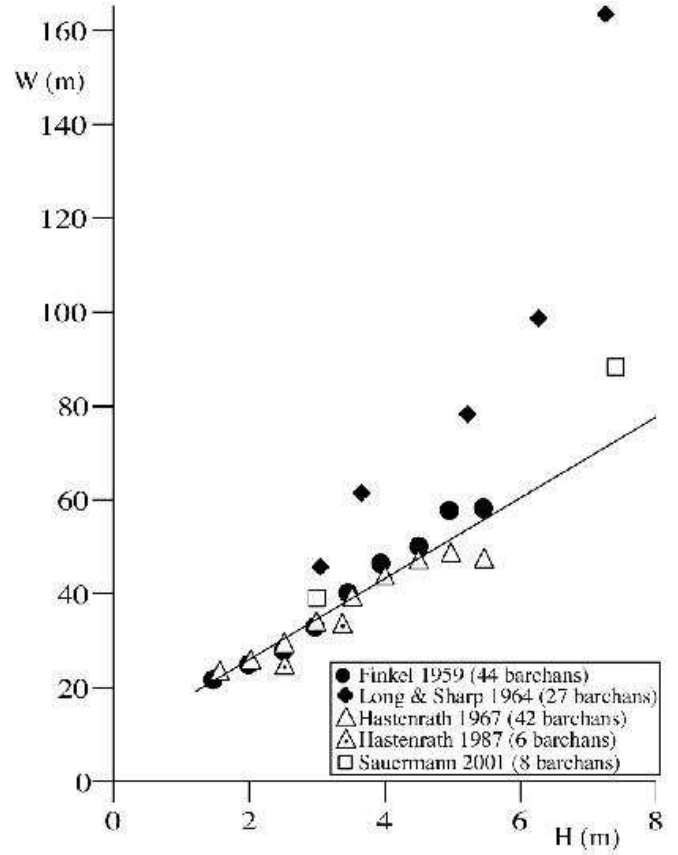


**Fig. 4.** Relationship between barchan width  $W$  and height  $H$  determined from field measurements averaged by ranges of heights. The solid line is the best linear fit to the points corresponding to barchans from the Arequipa region in Southern Peru (Finkel [3] and Hastenrath [6,9]).

### 2.1 Morphologic relationships and scale invariance

The crescent-like shape of the barchan is well known (see figures 1 and 2) and can be characterized by a few parameters, the length  $L$  along the central axis (which is also the wind direction), the height  $H$ , the width  $W$  and the horn length  $L_{horns}$  (see figure 2). Note that in practice, the two horns have always different lengths due to the fluctuations of wind direction. They are thus measured separately and averaged to give  $L_{horns}$ .

The region around La Joya in southern Peru is the most documented barchan field [3,6,9,22] and that for which measurements are the most coherent. Finkel [3] and later Hastenrath [6,9] have chosen a squared region, a few kilometres width, and have investigated systematically the morphologic parameters of the barchans in this perimeter. Their data exhibit a large statistical dispersion due to the variations of the control parameters on the field. Then, it is not surprising to find a dependence of the dune shape on the local conditions like the wind regime, the sand supply, the presence or not of other dunes in the vicinity, the nature of the soil, or whether the studied dunes have achieved a permanent state or are in a transient state...

Despite this strong dispersion of data, clear linear relationships between the height  $H$ , the length  $L$  and the width  $W$  (see figure 2) were found by Finkel [3] and Hastenrath [6], but with different coefficients ( $W = W_0 + \rho_W H$  and  $L = L_0 + \rho_L H$ ). To seek for relationships valid statistically, we follow the procedure of Finkel [3] and average all the measurements by ranges of heights (see figures 3 and 4). More precisely, we have considered the barchans between 1 m and 2 m high and averaged their length, width and height; this gives one point on figures 3 and 4. The same computation was done for the barchans between 1.5 m and 2.5 m, between 2 m and 3 m, etc. We can reasonably expect the statistical relations to be that which would have been obtained in controlled, reproducible conditions.

It can be observed that linear relationships between the length  $L$ , the width  $W$  and the height  $H$  are nonetheless recovered but are actually the same for the three sets of measurements (Finkel [3] and Hastenrath [6,9]) made in Southern Peru. The best linear fits give  $\rho_W = 8.6$  and  $\rho_L = 5.5$  corresponding to the mean proportions of barchans near La Joya. The most important point is that  $L$ ,  $H$  and  $W$  are not proportional. On the contrary, the coefficients  $L_0 = 10.8$  m and  $W_0 = 8.8$  m are comparable to the size of the smallest dunes. This means that small and large dunes are not homothetic: dunes of different heights have different shapes. In other words, *barchans are not scale invariant objects*. As a consequence, there should exist (at least) a typical lengthscale (related to  $L_0$  and  $W_0$ ) in the mechanisms leading to the dune propagation.

There are very few places in the world similar to the Arequipa region (southern Peru). They are usually touched by trade winds driven by oceanic anticyclones. Because these anticyclones are very stable, the winds are constant and often very strong. It is the case with the Peruvian and Chilean coasts, with coastal Namibia, with the Atlantic coast of the Sahara from Morocco to Senegal and with the northern shores of Western Australia. Morphologic measurements were conducted in some of the places where there is a constantly prevailing wind direction and a smooth ground surface: in Mauritania by Coursin [4], in California by Long and Sharp [5], and more recently in Namibia by Hesp and Hastings [11] and in southern Morocco (former Spanish Sahara) by Sauermann *et al.* [12]. In the later case, the authors have not measured the whole barchans in a given area but selected some which were isolated and symmetric. Unfortunately, in these works, the number of barchans is too small to determine precise morphologic relationships. But they are sufficient to indicate that the morphology depends on the dune field (see figures 3 and 4). Briefly, we know almost nothing on the parameters important for dunes morphology. It can depend on the grain size, the density of dunes, the sand supply, the wind strength, its changes of direction, etc.

For instance, it has been observed by Allen [23] that barchans have a smaller width  $W$  and more developed horns  $L_{horns}$  under strong winds than light ones. But Hastenrath have reported measurements which indicate a weak dependence of the shape on the wind strength. He

returned to southern Peru [9] after a light wind decade and observed that all the dunes had strongly decreased in size. He measured a second time the morphologic parameters of 6 barchans (dotted triangle on figures 3 and 4): the points are almost on the same line than previously.

Another example is the coincidence (or not) of the brink and the crest (see figure 2 for a definition of these words). Hastenrath [6] and Sauermann *et al.* [12] have observed that small dunes present a broad domed convexity around the crest, clearly separated from the brink as in figure 2, while large dunes have the crest straight to the brink as in figure 1. This is represented schematically on figure 10. However, it had been reported before [20] that there exist barchans of the same height in the same dune field presenting alternatively the separation or the coincidence of the brink and the crest. The difference lies perhaps in the selection of barchans to be studied (isolated or not, symmetrical or not, etc.).

The last morphologic relation between the mean length of the horns  $L_{horns}$  and the barchan height  $H$  (figure 5) is a nearly perfect relation of proportionality:  $L_{horns} \simeq 9.1 H$ . Even more striking, the relation is approximately the same for all the dune fields measured (in particular La Joya, Peru [3,6,9] and Imperial Valley, California [5], see figure 5). This suggests that the scaling law of the horns length could be simpler and more robust than that of the back dimensions.

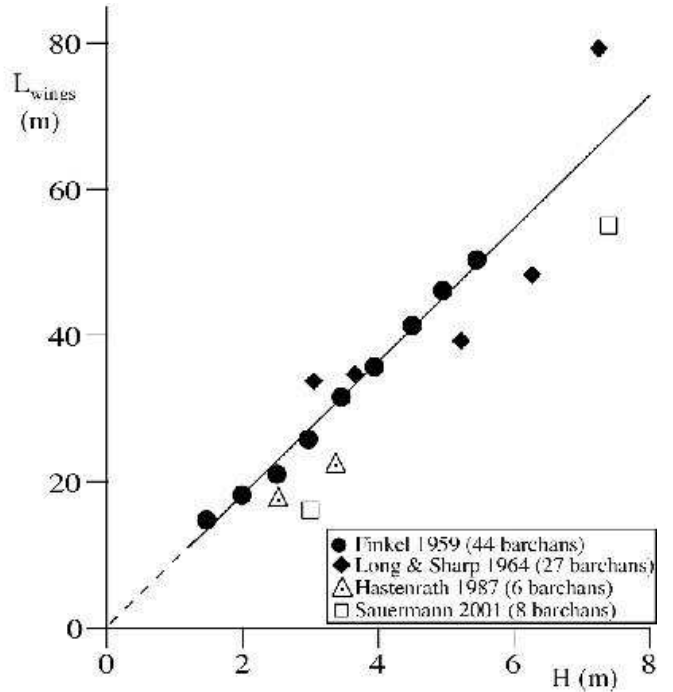


**Fig. 5.** Relationships between the horn length  $L_{horns}$  and the width  $W$  determined from field measurements averaged by ranges of heights. The solid line is the best linear fit to the points corresponding to barchans from the Arequipa region in Southern Peru (Finkel [3] and Hastenrath [6,9]).

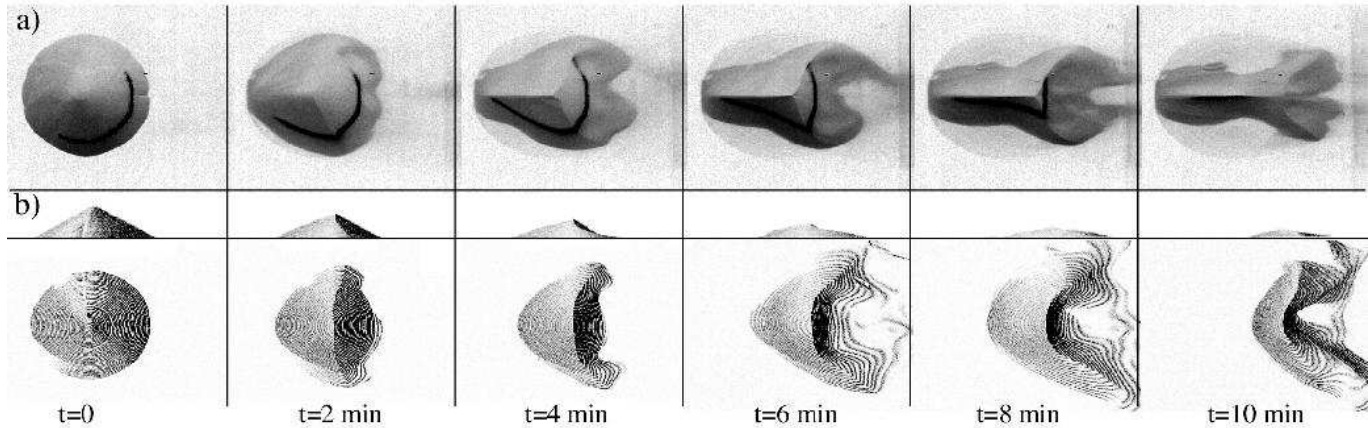


**Fig. 7.** Time evolution of a sandpile blown out by a controlled wind without (a) and with (b) a sand supply. In both cases the sandpile is eroded and disappears after a few minutes. Without sand supply, the erosion is localised on the sides so that a longitudinal brink is created. With a sand supply, the pile takes the form of a crescent. In particular, the back remains smooth and two horns grow by deposition of grains in reptation. In case b), both top and side views are shown. In particular, the initial height of the pile ( $\approx 20$  cm) can be seen.

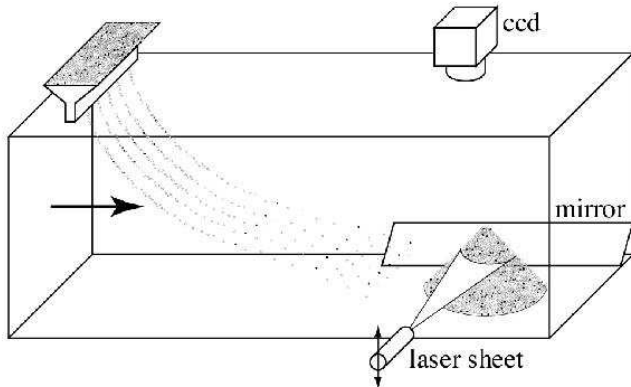


**Fig. 6.** To study the time evolution of a sandpile blown by the wind, the Cemagref wind tunnel (6 m long, 1 m large and 1 m high) was used. Pictures were taken from above using a video camera. A mirror was placed at  $45^\circ$  to get on the same picture a side view and a top view of the pile. The latter was enlightened by a lamp and by an horizontal laser sheet adjustable in height which reveals the topography. A tunable sand supply has been added at the top of the tunnel. The grains are PVC beads of size  $100 \mu\text{m}$ . The velocity (around  $6 \text{ m/s}$  at  $2 \text{ cm}$  above the soil covered by velvet) is chosen slightly above the threshold of motion of the grains.

## 2.2 Minimum size

It is striking to note the absence, on figures 3, 4 and 5, of measured dunes smaller than  $H = 1 \text{ m}$ ,  $W = 19 \text{ m}$  and  $L = 17.5 \text{ m}$ . This cut-off is clearly visible on the dune size histograms measured by Hastenrath [6]. Moreover, if barchans can be very thin sand patches in the region where they form, they are never lower than, say,  $1 \text{ m}$  in mature dunes regions. What happens to a small barchan? Related to this question, there have been several attempts [1,20,21] to generate an artificial dune from a small conical sandpile (typically  $10 \text{ cm}$  to  $1 \text{ m}$  high).

Here we report an experiment made in the Cemagref wind tunnel, described on figure 6. A conical sandpile  $20 \text{ cm}$  high is built from a funnel. It is then eroded by the air flow with (case b) or without (case a) a sand supply at the beginning of the wind tunnel (figure 7). Whatever the conditions (even with a sand supply), the pile loses mass inexorably, and disappears in a few minutes. This is also what was found in field experiments [1,20,21].

Figure 7 shows the evolution of the sandpile in the two cases, for a wind velocity chosen slightly above the threshold of motion of the grains. In case a), without a sand supply, the erosion is localised on the sides and the formation of a longitudinal brink is observed. In the last steps the side faces become so steep that avalanches occur. In case b), the input sand flux is tuned to be slightly below the saturated flux. Both the back and the sides are eroded so that the pile takes the form of a barchan. In particular, we observe the progressive formation of two horns due to the lateral deposition of grains in reptation.

The observation that a sandpile  $20 \text{ cm}$  high disappears whatever the conditions suggests that barchan dunes have a minimal size. This was first noticed by Bagnolds who interpreted the cut-off scale (the minimum dune size) as the saturation length which will be defined and discussed in details in section 3.3. Basically, it is the length over which the sand carrying increases when the wind passes from a firm soil to a sand patch. This interpretation has not been confirmed so far and deserves further investigations. Still the existence of a minimal size raises crucial problems. First, it means that no small size dune can be obtained in the air. Second, it asks a fundamental question: if a small barchan (or a conical small sandpile) is unstable and disappears after a short time, how then can barchans form?

## 2.3 Barchans velocity

In many places, barchans velocity has been measured [3, 2,4,5,6,9,10]. Typically, a small dune,  $3 \text{ m}$  high, propa-

gates at a speed ranging from 15 *m/year* to 60 *m/year* while this velocity is between 4 *m/year* and 15 *m/year* for a large dune, say 15 *m* high. Even though measurement points are very dispersed [20], there is no doubt that small dunes move faster than large ones.

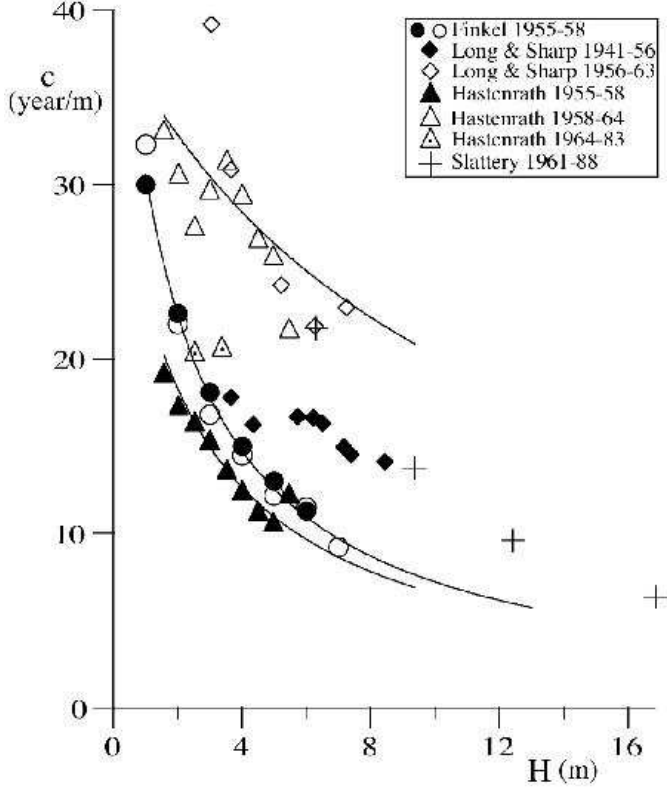


**Fig. 8.** Dune velocity, averaged by ranges of height, as a function of height. Solid lines correspond to the best fit of the data by a velocity of the form  $c = Q/(H_0 + H)$ . The fit is shown for the measurements in the Arequipa region (Finkel [3] and Hastenrath [6,9])

As for morphologic relationships, we have grouped the measurement points and averaged the velocity over several barchans. The resulting curves are shown on figure 8. It can be seen that the dune velocity is very different from one place to another. In the imperial valley, California, dune displacements were measured by Long & Sharp [5] from 1941 to 1956 (black diamonds), and from 1956 to 1963 (white diamonds). In Peru, they were measured by Hastenrath [6,9] from 1955 to 1958 (black triangle), from 1958 to 1964 (white triangle), and from 1964 to 1983 (dotted triangle). From these two data sets, it can be seen that barchan velocity  $c$  strongly depends on time. This is probably related to the fact that it obviously depends on fluctuating parameters like the wind speed or the sand supply.

However, in each dune field and especially in Southern Peru (figure 9), the relationship between velocity and size

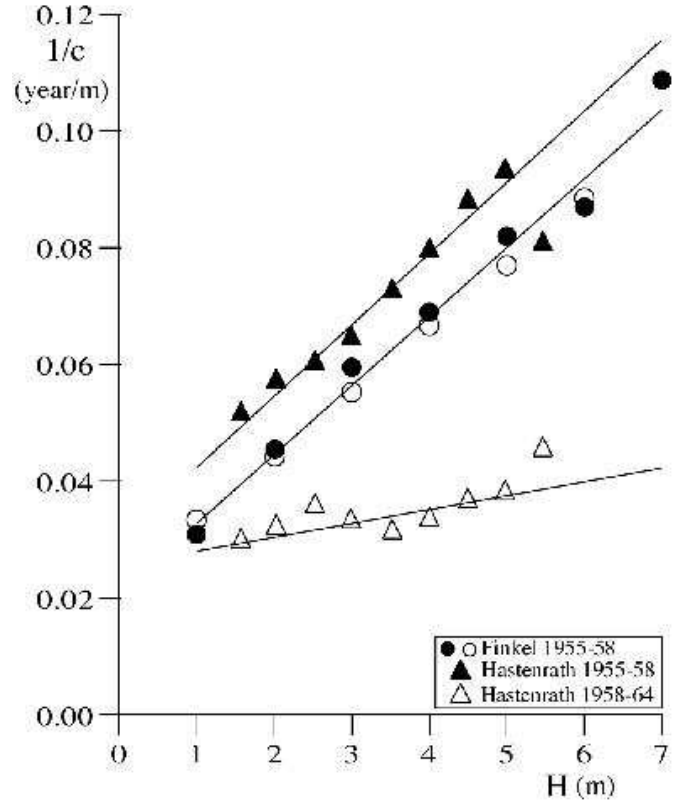


**Fig. 9.** Inverse dune velocity  $1/c$ , averaged by ranges of height, as a function of height  $H$ . Only the measurements made in the region of La Joya (Southern Peru) are shown.

can be reasonably described by:

$$c \simeq \frac{Q}{H_0 + H}. \quad (1)$$

This relation is represented schematically on figure 10.  $Q$ , which is homogeneous to a volumic sand flux, is found to be approximately equal to 85  $\text{m}^2/\text{year}$  between 1955 and 1958 and to 425  $\text{m}^2/\text{year}$  between 1958 and 1964, in southern Peru (figure 9).  $H_0$  is a cut-off height ranging from 1.8 *m* (Finkel 1955-58) to 10.9 *m* (Hastenrath 1958-64).

From the propagation speed, we can construct the dune turnover time  $T_{\text{turnover}}$  as the time taken by the dune to travel over its own length:

$$T_{\text{turnover}} = \frac{L}{c} \simeq \frac{L(H_0 + H)}{Q}. \quad (2)$$

It is also the typical period of the cycle of motion of a grain of the dune: erosion from the back, deposition at the top of the slip face, flowing in an avalanche, at rest below the dune, reappearance at the back of the dune, etc. It gives also the typical time needed by the dune to readjust its whole shape to changes of external conditions (wind, sand supply...). Typically, a small dune, 3 *m* high, has a turnover time between 5 *months* and 2 *years* while

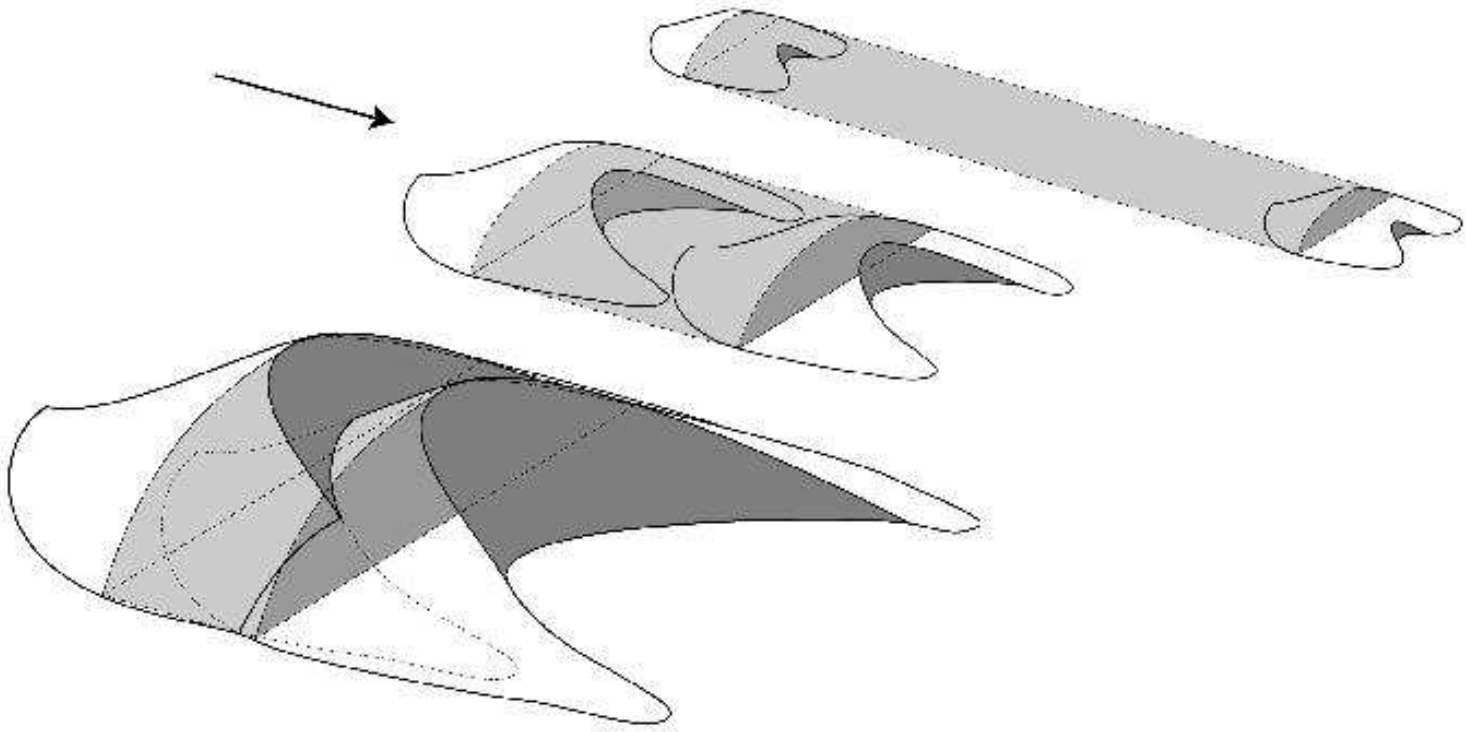


**Fig. 10.** Visual representation of the relation between the dune velocity  $c$  and its height  $H$ : three barchans are represented at initial time and after some time  $t$ . It can be seen that small dunes go faster than large ones. From the scalings of the speed  $c$  and the width  $W$  (see text), we can infer that the area  $W ct$  swept by the barchan (in light grey) is almost independent of the dune size. It can be seen on the large barchan that the back of the dune is eroded while the slip face and the horns are regions of sand deposition.

it ranges from 6 *years* to 25 *years* for a large dune, 15 *m* high. According to Oulehri [24], this large difference of turnover times between small and large dunes was already known in ancient times by saharan people. Barchans were used as cereal lofts or to protect goods from pillaging. A small or a large dune was chosen, function of the time after which they wanted to recover the bundle.

### 3 Mechanisms, dimensionless parameters and scaling laws

The previous field observations and measurements rise several questions. What are the basic dynamical mechanisms acting in the initiation and the propagation of barchans? What determines the equilibrium shape of barchans? Can we predict the morphologic relationships and the speed of dunes? Why is barchan shape not scale invariant?

The first part of this program i.e. the basic dynamical mechanisms, have been investigated in Bagnolds pioneering work [1]. We give here a complete overview of these mechanisms and we reformulate the corresponding scaling laws.

#### 3.1 Saltation and reptation

##### 3.1.1 Turbulent boundary layer

The dune dynamics is controlled by the sand transport which is itself driven by the wind. For a fully developed turbulent wind over a flat surface composed by grains of typical size  $d$ , the wind velocity  $u$  usually increases logarithmically with height  $z$  (see figure 11). This can be simply understood in the context of turbulent boundary layers theory. The standard turbulent closure relates the air shear stress  $\tau$  to the velocity gradient  $\partial_z u$ :

$$\tau = \rho_{air} \left( \kappa \frac{\partial u}{\partial \ln z} \right)^2 \quad (3)$$

where  $\rho_{air}$  is the volumic mass of air (see table 1) and  $\kappa \simeq 0.4$  is the Von Kármán constant. For a steady and uniform boundary layer, the shear stress  $\tau$  is constant and equal to  $\tau_0$ , the shear force per unit area on the bed. Besides, it turns out that the velocity vanishes at a distance  $rd$  from the sand bed. The rescaled bed roughness  $r$  is found to be of the order of  $1/30$  [1, 20]. This gives a logarithmic velocity profile, as observed on the field:

$$u(z) = \frac{u_*}{\kappa} \ln \frac{z}{rd}, \quad (4)$$

where the shear velocity  $u_*$  is by definition  $u_* = \sqrt{\tau_0 / \rho_{air}}$ . We will see in the following how the sand transport modifies this velocity profile.

### 3.1.2 Motion of one grain in the wind

A wind of sufficient strength can dislodge and entrain sand grains. Once they have taken off the sand bed, they are progressively accelerated by the wind, as they go up. The trajectories are observed to be asymmetrical, as shown on figure 11. The grains are submitted to the gravity and to the fluid drag force which leads to the standard following equation:

$$\frac{d\mathbf{v}}{dt} = \mathbf{g} + \chi \frac{\rho_{air}}{\rho_{sand}} \frac{|\mathbf{u} - \mathbf{v}|(\mathbf{u} - \mathbf{v})}{d} \quad (5)$$

where  $\mathbf{v}$  is the grain velocity,  $\rho_{sand}$  the volumic mass and  $\mathbf{u}$  the local wind velocity – which depends on  $z$ . The drag coefficient  $\chi$  depends on the shape of the grain but also on the Reynolds numbers  $Re = d|\mathbf{u} - \mathbf{v}|/\nu$  ( $\nu$  stands for the air viscosity). At large  $Re$ , in the turbulent regime,  $\chi$  tends towards a constant if the grain is sufficiently rough [27]. In the viscous – Stokes – regime,  $\chi$  decreases as  $1/Re$ .

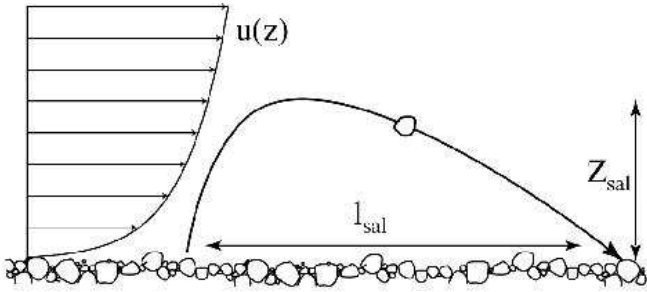


**Fig. 11.** In a fully turbulent boundary layer, the velocity profile is logarithmic. A grain dislodged from the bed is accelerated by the wind as it goes higher and higher and decelerated in the descent so that its typical trajectory is asymmetric. Saltation hop lengths  $l_{sal}$  are found to be about 12 to 15 times the height of bounce  $Z_{sal}$ .

In the vertical direction, the motion is dominated by gravity. It immediately follows, as for a free parabolic flight, that the flight time  $T$  and the height of bounce  $h$  depend on the launch speed  $w$  as:

$$T \propto \frac{w}{g}; \quad Z \propto \frac{w^2}{g}. \quad (6)$$

Note that, due to the quadratic drag force, these expressions must be corrected at strong winds [25]: the height of bounce  $Z$  get actually smaller than that of the free flight. These scalings are valid whatever the launch velocity  $w$  is. In the sequel we will distinguish between the different kinds of trajectories. For example, the indexes ‘sal’ and ‘rep’ will be used for saltation and reptation grains. If no label is specified, it means that the argument applies in general.

How does the flight time  $T$  compare with the timescale  $T_{drag}$  after which the grain has been accelerated by the

drag force up to the wind velocity? Using the equation of motion (5), we get:

$$T_{drag} \propto \frac{\rho_{sand} d}{\chi \rho_{air} u}, \quad (7)$$

For typical values of the parameters (table 1), the saltation flight time  $T_{sal}$  and the drag timescale  $T_{drag}$  turn out to be of the same order of magnitude. This means that grains – larger than  $100\mu m$  – are not much sensitive to the turbulent fluctuations of the wind but also that the horizontal velocity of the grain is not far from the mean wind velocity along the trajectory. The grain spends most of the flight time around the trajectory maximum ( $z \simeq Z$ ). As a consequence, the grains mean horizontal velocity should be approximately equal to the wind velocity  $u$  at this height. The horizontal displacement – the saltation length – is of the order of the flight time  $T$  times the mean horizontal velocity:

$$l \propto \frac{wu}{g}. \quad (8)$$

All the direct [1, 25] and indirect [26, 27] measurements as well as the models [1, 28, 29] are in agreement with this simple approach of grains trajectories. On the other hand, the scalings of  $Z$  and  $l$  with the wind shear velocity  $u_*$  and the grain diameter  $d$  are still controversial up to now. Mainly, the problems are the modification of the wind – and thus  $u$  – by the saltating grains and the mechanism by which the launch velocity  $w$  is selected. As from now, it can be argued that the fastest grains, which are said to be in saltation, bounce so high that the wind  $u$  at the trajectory maximum  $Z_{sal}$  is almost undisturbed by the rare grains to pass there. Their velocity, in particular the vertical component  $w$  after a collision, should thus scale as  $u_*$ . Taking  $w = u_*$ , as suggested by Owen [28], the height of bounce reads:

$$Z_{sal} \simeq \frac{u_*^2}{g}. \quad (9)$$

The horizontal velocity  $u$  (at  $z = Z_{sal}$ ) scales with  $u_*$  but with a non dimensional prefactor ( $u \simeq \xi u_*$ ) reflecting the logarithmic velocity profile:

$$\xi = \frac{1}{\kappa} \ln \left( \frac{u_*^2}{rgd} \right). \quad (10)$$

For those high energy grains, the saltation length,

$$l_{sal} \simeq \xi \frac{u_*^2}{g} \quad (11)$$

is  $\xi$  times larger than the saltation height  $Z_{sal}$  (figure 11). Experimentally [1, 25], the ratio  $l_{sal}/Z_{sal}$  is between 12 and 15, which is the order of magnitude found here for  $\xi$  (table 1). The grains bouncing the highest should thus have trajectories almost independent of their size  $d$  and scaling on  $u_*^2/g$  for the lengths and on  $u_*$  for the velocities.

**Table 1.** Definition and typical values of the main quantities discussed in the text.

Dune length	$L$	
Dune height	$H$	
Dune width	$W$	
Length of dune horns	$L_{horns}$	
Dune velocity	$c$	
Dune profile	$h(x, y, t)$	
Sand flux	$\mathbf{q}(x, y, t)$	
Rescaled roughness	$r$	1/30
Von Kármán constant	$\kappa$	0.4
Shear stress	$\tau$	
Air-borne shear stress	$\tau_{air}$	
Grain-borne shear stress	$\tau_{sand}$	
Quartz density	$\rho_{sand}$	2650 kg.m <sup>-3</sup>
Grain diameter	$d$	200 $\mu$ m
Shear velocity	$u_*$	0.5 m.s <sup>-1</sup>
Logarithmic velocity prefactor	$\xi$	20
Wind velocity	$u$	10 m.s <sup>-1</sup>
Saltation flight time	$T_{sal}$	50 ms
Saltation hop height	$Z_{sal}$	2.5 cm
Saltation hop length	$l_{sal}$	50 cm
Reptation hop length	$l_{rep}$	8 mm
Static friction coefficient	$\mu_s$	$\tan(33^\circ) \simeq 0.65$
Dynamic friction coefficient	$\mu_d$	$\tan(31^\circ) \simeq 0.60$
Air density	$\rho_{fluid}$	1.2 kg.m <sup>-3</sup>
Air viscosity	$\nu$	1.5 10 <sup>-5</sup> m <sup>2</sup> .s <sup>-1</sup>
Grain Reynolds number	$Re$	$du_*/\nu \simeq 120$ $du/\nu \simeq 2500$
Impact threshold velocity	$u_{imp}$	15 cm.s <sup>-1</sup>
Fluid threshold velocity	$u_{flu}$	20 cm.s <sup>-1</sup>
Saturated sand flux	$q_{sat}$	180 m <sup>2</sup> /year
Drag time	$T_{drag}$	50 ms
Drag length	$l_{drag}$	9 m
Reptation flux	$q_{rep}$	
Vertical sand flux	$\phi$	
Number of splashed grains	$N_{eje}$	

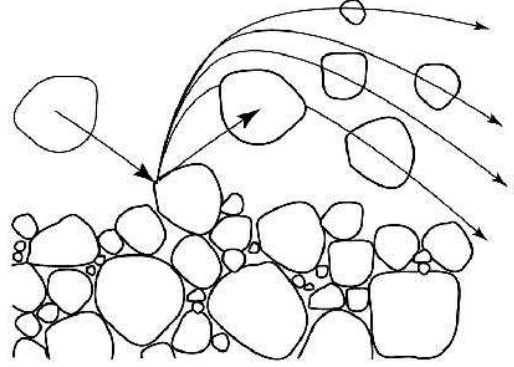
### 3.1.3 Collision of one grain on the sand bed

When a saltating grain collides the sand bed, it rebounds but can also eject other grains (figure 12). In general, the rebounding grain differs sufficiently from the ejected grains to be recognised. However, there are low probability configurations for which the incident grain delivers its momentum to few nearby grains but remains trapped, even for large impact velocities. The non dimensional parameter which controls the rebound probability  $p_{reb}$  is the ratio of the impact velocity  $v_{imp}$  to the velocity necessary to escape from the potential trapping at the sand bed surface [30], namely  $\sqrt{gd}$ . In particular  $p_{reb}$  vanishes when  $v_{imp}$  becomes smaller than this escape velocity. The rebound probability resulting from the numerical simulation of Anderson and Haff [31,32] can be expressed as:

$$p_{reb} = p_\infty \left[ 1 - \exp \left( -\frac{v_{imp}}{a\sqrt{gd}} \right) \right] \quad (12)$$

$p_\infty \simeq 0.95$  is the rebound probability for velocities much larger than  $a\sqrt{gd}$ .  $a$  is a non-dimensional number equal to 10 in Anderson and Haff two-dimensional simulations [31, 32].

Experiments [25,33] and numerical simulations [31,32] show that the rebound velocity  $v_{reb}$  is a fraction of the impact velocity  $v_{imp}$ :  $v_{reb} = \gamma v_{imp}$ . The restitution coefficient  $\gamma$  is around 0.5. The rebound angle  $\theta_{reb}$  is almost independent of the impact velocity (modulus and angle) and ranges from 35° to 50°.

**Fig. 12.** When a saltating grain collides the sand bed, it rebounds and splashes up other grains.

The characteristics of the ejecta are also well documented [31,32,33]. The distribution of the ejection velocity – both the modulus  $v_{eje}$  and the angle  $\theta_{eje}$  from the horizontal – is found to be almost independent of the impact velocity  $v_{imp}$ . The mean ejection speed is related to the escape velocity  $\sqrt{gd}$ :

$$v_{eje} \simeq a\sqrt{gd} \quad \text{and} \quad \theta_{eje} \simeq 70^\circ \quad (13)$$

A constant fraction of the impact momentum is transferred to the ejecta so that, on the average, the number of ejecta increases linearly with the impact speed:

$$N_{eje} = \frac{v_{imp}}{a\sqrt{gd}} - 1 \quad \text{if } v_{imp} > a\sqrt{gd} \quad (14)$$

Again, the same critical velocity  $a\sqrt{gd}$  appears. It is at the same time the critical velocity below which no grain is on the average ejected, the mean ejection speed and the velocity below which the rebound probability strongly decreases.

These low energy grains ejected from the sand bed move near the surface of the sand bed: they bounce typically at a few hundred times the grain size. Such grains are said to be in reptation [34], in contrast with saltation which relates to high energy bouncing grains transported by the wind. The reptation is at the origin of the formation of ripples which, by the way, propagate and thus also takes part in the sand transport.



### 3.1.4 Saltation versus reptation

The slowest grains, the ‘reptons’, have properties that depend only on the grain size: the bouncing height scales with  $d$  and the grain velocity with  $\sqrt{gd}$ . On the other hand, the fastest grains, the ‘saltons’, have properties which depend mainly on the shear velocity  $u_*$ . Between the two, there is a continuum of trajectories of different jump lengths which all contribute to the sand flux [32,38,39]. Experimentally, this can be observed directly or deduced from the fact that the sand transport is a continuous function of height. Why then making a distinction between reptation and saltation?

The first answer is of course that the two limit trajectories – slowest and fastest – of the distribution do not present the same scaling. Let us turn to the experiment presented in section 2.2 (figures 6 and 7) which clearly illustrates the difference. For any wind velocity above the threshold of motion of the grains, the saltation length is larger than the size of the pile (typically 1 m compared to 40 cm): no saltating grain dislodged from the pile is deposited on it. As a consequence, the pile is only eroded. Then it is surprising to observe on figure 7 the formation of horns, downwind the initial position of the pile. This means that they have been formed by grains deposited there which can only be grains in reptation. The whole figure 7 can be read in this way: the pile is eroded due to saltation but the formation of a crescent shape in particular the horns are due to reptation. In this situation, the flux of grains in saltation (visible by the overall leak of matter) and the flux of grains in reptation (visible by the formation of horns) are comparable.

As indicated by experiments [36,38,39] and numerical simulations [31,32] the sand transport is maximum at the ground level and decreases exponentially with height. Thus, the contribution of reptons to the overall flux of sand should be important. The ratio between saltation and reptation fluxes has only been measured directly by Bagnolds [1] using two different traps: a rectangular trap was placed vertically for the saltons and a second one, with a thin linear mouth, was buried in the soil to trap the grains moving just at the surface. In fact this hole could only trap the slowest and largest reptons. Bagnolds proposed to designate this motion by surface creep. Anderson, Sørensen and Willetts [34] gave a more precise definition of creeping grains as grains which get rearranged by saltation impacts and which are not affected directly by wind forces. This category is actually useful for binary mixtures [1], to describe the motion of the heavy grains submitted to a rain of light ones. With these traps, Bagnolds found that the creeping flux was only three to four times smaller than the saltation flux.

Since the grains in reptation are dragged along by saltating grains, we can infer that the reptation flux is just proportional to the saltation flux. Defining the vertical flux  $\phi$  as the volume of particles leaving the soil per unit time and unit area, the reptation flux  $\phi_{rep}$  is governed by the splash of saltation grains. In first approximation,

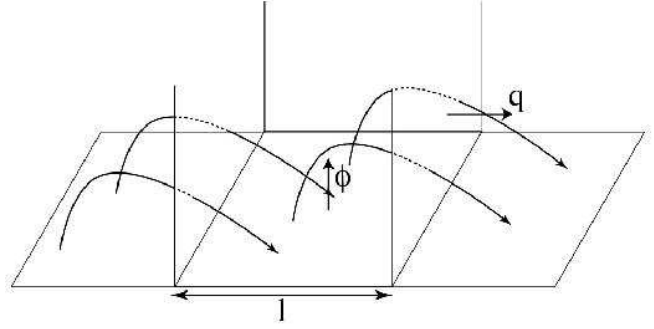


**Fig. 13.** The flux  $q$  is the volume of sand which crosses a unit line transverse to the wind per unit time. If the typical path of a grain has a hop length  $l$ , the incident flux of grains  $\phi$ , which is the volume of grains colliding a unit area per unit time, is equal to  $q/l$ .

this can be written as:

$$\phi_{rep} = N_{eje} \phi_{sal} \quad (15)$$

Because  $N_{eje}$  increases linearly with  $u_*/\sqrt{gd}$ , the number of reptons leaving the soil per unit time is much larger than the number of saltons. For the sand transport, the important quantity is the flux  $q$  defined as the volume of sand crossing a unit line transverse to the wind per unit time (figure 13). The relation between the vertical flux  $\phi$  and the integrated horizontal flux  $q$  is determined by the grains typical hop length  $l$ . For the grains in saltation, this gives:

$$q_{sal} = \phi_{sal} l_{sal} \quad (16)$$

Then the relation (15) between fluxes of saltation and reptation can be expressed in terms of  $q$ :

$$q_{rep} = \frac{l_{rep} N_{eje}}{l_{sal}} q_{sal} \quad (17)$$

Since  $l_{rep}/l_{sal}$  decreases as  $gd/u_*^2$ , this means that the contribution of reptons to the overall flux of sand decreases with the wind velocity. This is consistent with the disappearance of ripples at large wind. One should thus be very careful in identifying the species most important for the sand flux: the result is opposite for the horizontal flux  $q$  and the vertical flux  $\phi$ . Finally, the same question can be risen: if the two fluxes are proportional one with the other, why making a distinction between the two?

Another important difference appears when the sand bed presents a slope, in particular if the steepest slope is perpendicular to the wind. Howard [40] have observed that the normal to ripples are no more parallel to the wind on sloping surfaces but are deflected downslope by as much as  $35^\circ$ . This clearly shows that the gravity force has an influence on the direction of motion of reptons. Moreover, Howard [40] found a good agreement with a simple calculation considering that the ejected grains are submitted to an effective drag along the wind direction, just sufficient to escape from potential trapping. Most of their flight, saltons are dragged along the wind direction

but their rebound direction could be influenced by the surface slope.

More recently, Hardisty and Whitehouse [41] have shown that the bedslope along the direction of motion modifies the threshold of motion (typically 15% for a  $10^\circ$  slope) but also the flux itself. They found that the flux was multiplied by 10 for a  $10^\circ$  downslope and divided by 6 for a  $10^\circ$  upslope. These very striking results were not confirmed by Rasmussen and Iversen [38,39,42] who have found a much weaker dependence of the saturated saltation flux with the longitudinal slope.

There still misses experimental studies investigating the dependence of the reptation flux with the slope – in particular a lateral slope. Still, it can be argued that gravity is important in the ejection process. The number of ejecta should be smaller for a positive slope along the wind direction than for a negative slope and reptons should be deflected downslope by gravity. Then, the total flux is not aligned along the direction of wind but has a component along the steepest slope. To the first order this downslope flux is simply proportional to the gradient  $\nabla h$  of the quantity transported (the local height  $h$ ). It thus leads to diffusive effects which tend to smooth the dune.

### 3.2 Entrainment by the fluid and by impacts

#### 3.2.1 Fluid threshold

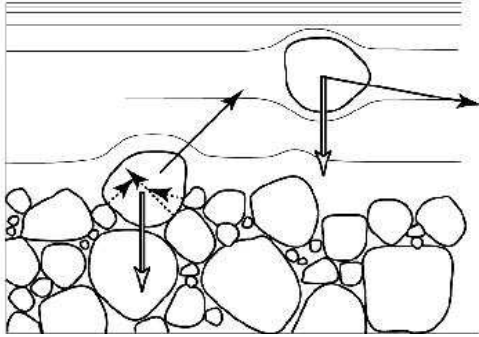


**Fig. 14.** Wind is accelerated over grains at the surface of the sand bed. To lift up a grain, the low pressure created by the wind flow has to be larger than gravity. There is thus a threshold velocity below which the wind can not erode the sand bed.

It is somewhat striking that grains can be dislodged by the wind since they fall down again after having taken off. This is due to the asymmetry of the flow around a static grain at the surface of the sand bed, as demonstrated by figure 14. Since  $\tau$  is by definition the horizontal force per unit area, the drag force acting on a grain at the surface of the sand bed scales as  $\tau_0 d^2$ . A grain will escape from trapping only if this force is larger than gravity. As a consequence, there exists a threshold shear velocity  $u_{flu}$  below which a sand bed at rest cannot be eroded by the

**Table 2.** Typical values of the quantities defined and discussed in the text. The aeolian sand transport is compared to that in water.

Fluid	Air	Water
$\rho_{fluid}$	$1.2 \text{ kg.m}^{-3}$	$1000 \text{ kg.m}^{-3}$
$\nu$	$1.5 \cdot 10^{-5} \text{ m}^2.\text{s}^{-1}$	$10^{-6} \text{ m}^2.\text{s}^{-1}$
$Re_* = du_*/\nu$	120	8
$Re = du/\nu$	2500	170
$u_{imp}$	$15 \text{ cm.s}^{-1}$	$15 \text{ cm.s}^{-1}$
$u_{flu}$	$20 \text{ cm.s}^{-1}$	$0.7 \text{ cm.s}^{-1}$
$q_{sat}$	$180 \text{ m}^2/\text{year}$	$17 \text{ m}^2/\text{hour}$
$T_{drag}$	$50 \text{ ms}$	$0.1 \text{ ms}$
$l_{drag}$	$9 \text{ m}$	$1 \text{ cm}$

wind:

$$u_{flu} = \zeta_{flu} \sqrt{\frac{\rho_{sand} - \rho_{air}}{\rho_{air}} gd}. \quad (18)$$

Experimentally, the rescaled threshold velocity  $\zeta_{flu}$  is found to be around 0.1 (see table 1).

Above  $u_{flu}$  grains spontaneously start rolling at the surface of the sand bed [44]. During their motion, some grains can take off the bed, due to the bumps beneath them or to the aerodynamic lift force. As soon as they have left the bed, the flow around them become again symmetric (figure 14) so that they start being accelerated downward by gravity. They collide the bed, rebound and eject other grains. The later are accelerated by the wind, splash on the sand bed and so on, until saturation be reached (see part 3.3).

#### 3.2.2 Impact threshold

Suppose that there are already some grains in saltation. If the wind velocity decreases, the grains velocity also decreases. So does the sand flux. The minimum wind velocity which can sustain the sand transport is that for which the grains impact velocity is no more sufficient to eject other grains (see section 3.1.3). This happens for  $v_{imp} \simeq a\sqrt{gd}$  and thus for a wind velocity  $u_*$  of the order of a few times  $\sqrt{gd}$ :

$$u_{imp} = \zeta_{imp} \sqrt{gd}. \quad (19)$$

Experimentally, the rescaled threshold velocity  $\zeta_{imp}$  is found to be around 3.5 (see table 1).

#### 3.2.3 Entrainment by the fluid and by impacts

In the case of aeolian sand transport, we see on table 2 that the ‘impact’ threshold velocity is smaller than the ‘fluid’ threshold velocity. This means that the transition from the sand bed at rest to the saturated sand transport presents a hysteresis. Starting from a light wind ( $u_*$  smaller than both  $u_{imp}$  and  $u_{flu}$ ), the sand flux is null. Then, if the wind velocity increases above the fluid threshold  $u_{flu}$ , the grains start being entrained directly by the wind and a saturated sand transport establishes. Now, if

the wind velocity decreases, the sand flux vanishes at  $u_{imp}$  only. This is characteristic of a subcritical transition. The consequences of this hysteretic behaviour has not been investigated, so far.

From this point of view, the sand transport behaves very differently in liquids. It can be seen on table 2 that the fluid threshold velocity in water is much smaller than the impact threshold. This means that the hysteresis disappears in water – as in liquids in general. It also indicates that the sand transport under water is dominated by direct fluid entrainment, due to the favourable density ratio. By comparison, the splash process is inefficient and there is, so to say, no saltation – and therefore no reptation – under water.

In order to distinguish the direct entrainment of grains by the fluid from saltation and reptation, we propose the name ‘traction’ for this motion. This word is derived from the latin verb *trahere* which means to drag<sup>1</sup>. ‘Tractions’ are thus the predominant species under water. Traction is very similar to avalanches except that the driving mechanism is the fluid drag instead of the gravity. Then, the same kind of description could in principle be adapted (see section 3.5).

### 3.3 Saturated flux and saturation length

#### 3.3.1 Negative feedback on the wind

The only limit to the erosion of a sand patch is the saturation of the sand flux. It occurs because of the negative feedback of the transported sand on the wind strength. The point is that the same momentum flux is used to maintain the turbulent boundary layer and to speed up the entrained grains. For a given shear velocity, there is thus a maximum flux of sand, called the saturated flux  $q_{sat}$ , which can be transported by the wind.

Since they are accelerated by the wind, the grains, at a height  $z$ , have a smaller velocity  $u_{\uparrow}$  when they go up than when they come down again ( $u_{\downarrow}$ ). The volume of sand which collides a unit area of the sand bed per unit time is, by definition, the flux  $\phi$ . As shown on figure 13, it is related to the horizontal flux  $q$  integrated along the vertical and to the hop length  $l$ :  $\phi = q/l$ . The momentum transferred to this volume of sand is by definition the sand-borne shear stress  $\tau_{sand}$  and is equal to the mass flux  $\rho_{sand} \phi$  times the velocity difference  $u_{\uparrow} - u_{\downarrow}$ :

$$\tau_{sand} = \rho_{sand} \phi (u_{\uparrow} - u_{\downarrow}) \quad (20)$$

The remaining part of the total shear stress, the air-borne shear stress  $\tau_{air} = \tau_0 - \tau_{sand}$ , accelerates the flow itself. Assuming that the turbulent boundary layer is still at equilibrium, the standard turbulent closure (3) leads a modified velocity profile given by:

$$\frac{\partial u}{\partial \ln z} = \frac{1}{\kappa} \sqrt{u_*^2 - \frac{\rho_{sand}}{\rho_{air}} \phi (u_{\uparrow} - u_{\downarrow})} \quad (21)$$

<sup>1</sup> *Saxa ingentia fluctus trahunt* (De bello Jugurthino, Sallustius), i.e. huge stones are dragged by the flow.

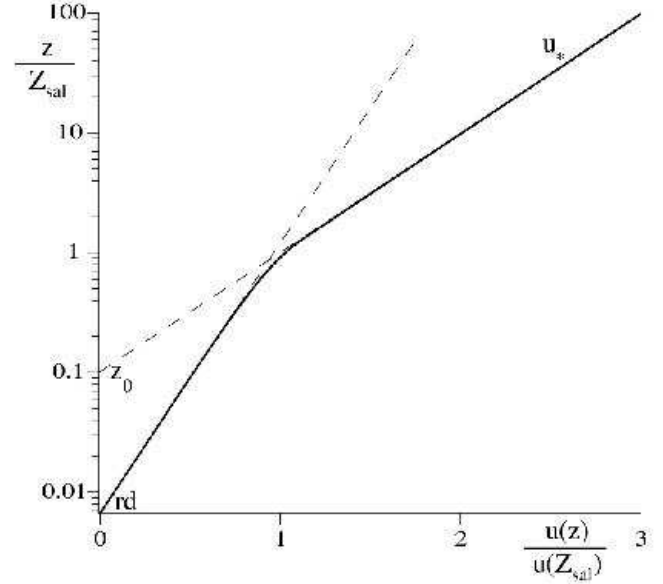


**Fig. 15.** Velocity profile modified by the sand transport, as obtained theoretically by Owen [28] and Raupach [43] and in numerical simulations by Anderson and Haff [31, 32]. It is a piecewise logarithmic profile. Inside the saltation layer ( $z/Z_{sal} < 1$ ), the shear velocity is decreased but the roughness ( $rd$ ) is that of the bed. Outside ( $z > Z_{sal}$ ), the shear velocity is  $u_*$  but the apparent roughness  $z_0$  has increased, as if the soil was higher.

with the same boundary condition than previously,  $u = 0$  at the height  $z = rd$ .

Above the saltation layer, there is no grain and thus no grain-borne shear stress:  $\tau_{air} = \tau_0$ . An undisturbed turbulent boundary layer is thus recovered, but with an increased apparent roughness  $z_0$  (figure 15). Everything looks as if the soil has been risen at a height  $z_0 - rd$ . Just above the soil, inside the reptation layer, the air-borne shear stress  $\tau_{air}$  is strongly reduced, and is much smaller than  $\tau_0$ . As a consequence, the roughness is similar ( $u$  vanishes at  $rd$ ) but the apparent shear velocity is smaller than  $u_*$  (figure 15). Experimentally, the velocity profile is found to be logarithmic, with an increased apparent roughness  $z_0$ , but the lowest part of the profile is too thin to be measured [1, 25, 38, 39, 42]. Therefore, the numerical and theoretical findings for the velocity profile inside the saltation layer should be checked experimentally.

#### 3.3.2 Equilibrium transport

In the previous sections, only the consensual properties of sand transport have been reviewed. We now come – in this subsection – to the controversial points.

It is clear that the hop height depends on the launch velocity  $w$  and scales as  $w^2/g$ . The hop length depends on  $w$  and on the mean horizontal velocity  $u$ , and scales as  $wu/g$ . Now, what are the mean velocity components  $u$  and  $w$  when the equilibrium is achieved? Nalpanis *et*

*al.* [25] have found that the mean vertical launch velocity  $w$  is about  $2u_*$  and that both  $h$  and  $l$  scale on  $u_*^2/g$ . On the other hand, Rasmussen and Iversen [38, 39, 42] have reported measurements of the horizontal grain speed showing almost no dependence of  $u$  on the shear velocity  $u_*$ . The scaling found by Nalpanis & al. [25] is that of the saltons while the scaling found by Rasmussen and Iversen [38, 39, 42] corresponds to the reptons. A third scaling has been obtained by Jensen and Sorensen [26, 27] who have used a model to extract the same quantities from experimental measurements of the vertical variation of the transport rate.

Another – indirect – measurement has also been conducted by Rasmussen and Iversen [38, 39, 42]: they have studied systematically the dependence of the apparent roughness  $z_0$  with the wind velocity  $u_*$  and the grain size  $d$ . From figure 15, it can be inferred that  $z_0$  is related to the height of bounce  $Z$  [43] and to the mean horizontal velocity  $u$  ( $\simeq u(Z)$ ) by  $z_0 = Z \exp(-u(Z)/u_*)$ . If  $w$  and  $u$  scale as  $u_*$ ,  $z_0$  should scale as  $u_*^2/g$ . If  $w$  and  $u$  are independent of  $u_*$ ,  $z_0$  should increase with  $u_*$  and saturate at a value independent of  $u_*$ . The experimental measurements can be rescaled to give approximately:

$$z_0 \simeq r \left( \frac{u_*^2}{g} + (1 - \zeta_{imp})d \right) \quad (22)$$

The apparent roughness  $z_0$  tends to the soil roughness  $rd$  at the impact threshold and above, increases and scales asymptotically as  $u_*^2/g$ . According to the previous analysis, this means that the feedback of the sand transport on the wind is dominated by high energy grains.

As a conclusion, the question of the trajectory mean properties is not completely solved, perhaps because it is ill posed. It is clear that there is a distribution of characteristics ranging from the low energy reptons to the high energy saltons. Then, the scaling laws obviously depend on the way quantities are averaged. For instance, the result will be different if an average is weighted by the vertical flux, by the grain density, by the horizontal flux or even by the energy flux. Also the result will depend on the height of the lowest trajectory taken into account in the statistics, for instance when a camera is used.

### 3.3.3 Saturated flux

The saturation of the sand flux can be understood without entering in the details of the mechanisms. The first idea, proposed by Bagnold [1], was that equilibrium is reached when the sand-borne shear stress has taken a given part of the overall shear stress:  $\tau_{sand} \propto \tau_0 = \rho_{air} u_*^2$ . Replacing  $\phi$  by  $q/l$  in equation (20), we get:

$$q_{sat} \propto \frac{\rho_{air}}{\rho_{sand}} \frac{u_*^2 l}{u_{\uparrow} - u_{\downarrow}} \quad (23)$$

The hop length  $l$  scales as  $uw/g$ . The velocity difference between the rise and the descent  $u_{\uparrow} - u_{\downarrow}$  should be a fraction of the grain horizontal velocity  $u$ . This gives

$$q_{sat} \propto \frac{\rho_{air}}{\rho_{sand}} \frac{wu_*^2}{g} \quad \text{if } u_* > u_{imp}$$

$$q_{sat} = 0 \quad \text{if } u_* < u_{imp} \quad (24)$$

Owen [28] have introduced a refined argument: the saturation is reached when the wind shear velocity inside the saltation layer has decreased to its threshold value. In Owen's article, this threshold was  $u_{flu}$ , meaning that the erosion is due – and limited – by the direct aerodynamic entrainment. It seems more reasonable to use the impact threshold  $u_{imp}$ . Since  $\tau_{sand} = \tau_0 - \tau_{air} = \rho_{air} u_*^2 - \zeta_{imp} g d$ , this gives:

$$q_{sat} \propto \frac{\rho_{air}}{\rho_{sand}} w \left( \frac{u_*^2}{g} - \zeta_{imp} d \right) \quad (25)$$

More detailed formulas have been proposed for this relation [35, 29, 45] which, as this one, essentially smooth the Bagnolds relation around the threshold velocity  $u_{imp}$ .

Both expressions (24) and (25) depend on the typical launch velocity  $w$  which, as seen in the previous section, remains problematic. Nevertheless, we can conclude on the scaling of the saturated flux. First, the flux  $q_{sat}$  associated to high energy saltons ( $w \propto u_*$ ) increases more rapidly than the flux associated to low energy reptons ( $w \propto \sqrt{gd}$ ). Second, to maintain a possible saturated reptation flux, a saltation flux is needed, given by equation (17). For large shear velocity, the non dimensional factor  $l_{sal}/(l_{rep} N_{eje})$  relating  $q_{rep}$  to  $q_{sal}$  scales as  $u_*/\sqrt{gd}$ . So, to maintain a flux saturated by reptons, a flux of saltons scaling as  $\rho_{air}/\rho_{sand} u_*^3/g$  is needed. In any case, this is the scaling expected at large shear velocity even if reptons can be predominant just above the threshold. The last – and the best – argument is that  $q_{sat} \propto u_*^3$  is the scaling measured experimentally [1, 35, 36, 37], with a prefactor of order unity.

The expression (25) predicts that the saturated flux should slightly decrease for an increasing grain diameter  $d$ , due to the threshold effect. From experimental measurements, Bagnolds [1] has reported an increase of  $q_{sat}$  with  $d$ : for grains ranging from  $100 \mu m$  to  $1 mm$ , the prefactor in equation (24) is found to be  $\sqrt{d/D}$  with a new length  $D \simeq 150 \mu m$ . This is very striking since  $D$  should neither depend on  $u_*$  nor on  $d$ . Rasmussen and Iversen [38, 39, 42] have also an extra length in the scaling of the apparent roughness  $z_0$ . Introducing the same length  $D \simeq 150 \mu m$ , the fit of their data by

$$z_0 \simeq r \sqrt{D/d} \left( \frac{u_*^2}{g} + (1 - \zeta_{imp})d \right) \quad (26)$$

is much better than with expression (22). And again,  $D$  should neither depend on  $d$  nor on  $u_*$ . This new parameter  $D$  have to be related to the fluid entrainment (with a Reynolds number dependence) or to the collision process (with a dependence on the elastic properties of the material). This implies the existence of new mechanisms, not investigated so far.

### 3.3.4 Space and time lag

When the wind arrives at the edge of a sand sheet, it dislodges and carries away sand grains. The later fall down

again and eject other grains so that the transport rate increases. In turn, these grains in saltation reacts on the turbulent boundary layer to decrease the velocity. There is thus a lag between the edge of the sand sheet and the achievement of the sand flux saturation. This was first reported by Bagnolds [1] who observed experimentally that the transport rate of sand nonetheless increases towards its saturated value but overshoots and exhibits a damped oscillation in space. Other experimental papers report space lags but none have recovered the oscillation. The existence of a lag was recovered in the numerical simulation by Anderson & Haff [31,32]. Several authors have observed that the space lag before saturation – the saturation length – is almost independent of the shear velocity  $u_*$ , contrarily to the saltation length. Note that in cellular automaton models [14,15,17], there is also a lag but due to transport non locality i.e. to the fact that grains moves by jumps of one saltation length  $l_{sal}$ .

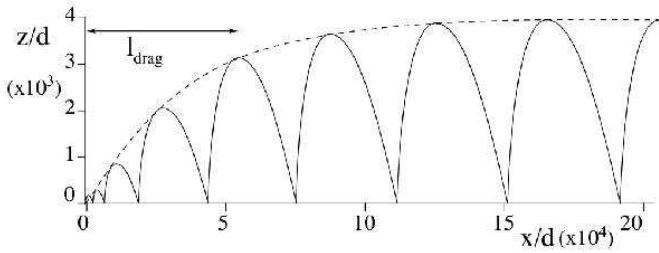


**Fig. 16.** Sketch of the promotion of a repton to saltation. Once ejected the grain reaches the wind velocity after a typical length  $l_{drag}$ . The equilibrium sand transport is achieved when the wind speed has so decreased that the number of reptons promoted to saltation is just equal to the number of saltions absorbed by the sand bed at their impact.

The physical mechanisms which lead to the sand transport equilibrium have not to be specified to derive the saturated flux. It is the interest of Bagnolds and Owen arguments but also their limits. But to understand the origin of the saturation length, these mechanisms have to be made explicit. Owen [28] have proposed a first idea: the flux saturates when the wind does not directly entrain grains any more i.e. when the wind shear velocity inside the saltation layer has decreased to its threshold value  $u_{flu}$ . It is probably the case for the sand transport in water but not in air, in which the direct aerodynamic entrainment is much less efficient than the entrainment by impacts.

Anderson & Haff [31,32] characterise the production of new grains in saltation by the mean replacement rate  $\eta$  which is the mean number of grains dislodged by an impacting grain (except itself, which rebounds). The flux saturates when the wind and thus the grains velocity becomes so small that  $\eta$  vanishes. The erosion rate which is the difference between the flux of grains taking off the bed and the flux of grains impacting on it, is given by the spatial derivative of the sand flux  $\partial_x q_{sal}$ . It is equal to the incident flux of grain  $\phi_{sal} = q_{sal}/l_{sal}$  times the mean

replacement rate  $\eta$ :

$$\partial_x q_{sal} = \eta \frac{q_{sal}}{l_{sal}} \quad (27)$$

The simplest possibility is to imagine, as proposed by Sørensen [29], that the ejected grains are of the same species than the impacting ones.  $\eta$  is then simply the number of ejected grains  $N_{eje}$  described by the equation (14). The saturation is reached when  $N_{eje}$  vanishes. This happens when all these saltions have a velocity of the order of  $a\sqrt{gd}$  – independent of  $u_*$  – i.e. when they have become reptons (figure 15). Because each grain gives  $1 + N_{eje}$  grains after a collision, the flux first increases exponentially with a typical lengthscale  $l_{sat} = l_{eje}$  equal to the saltation length  $l_{sal}$  divided by the typical replacement rate  $\eta$ :

$$l_{eje} \simeq ad \frac{u_*}{\sqrt{gd}}. \quad (28)$$

This equilibrium situation with a uniform reptation layer is far too simplified. If a grain jumps just above this layer, it is progressively accelerated and becomes a saltion, as seen on figure 16: the uniform reptation layer is unstable. Second, low energy grains have a large probability  $1 - p_{reb}$  to be absorbed by the sand bed when they collide it (eq. 12). At equilibrium, this should be balanced by a production of reptons. This suggests a slightly different picture in which saltions and reptons coexist pacifically. The saltions produce reptons when they collide the sand bed. reptons are promoted to the rank of saltions, once accelerated by the wind (figure 16). This is probably the situation reached in Anderson & Haff numerical simulation [31,32]. The production of reptons involves the typical length scale  $l_{eje}$  defined above. The acceleration of reptons to the velocity of saltions takes a length  $l_{drag}$  scaling on the grain size and on the sand to fluid density ratio:

$$l_{drag} \simeq \xi \frac{\rho_{sand}}{\rho_{air}} d \quad (29)$$

As time – and space – goes by, the reptation and saltation flux increase and the wind strength decreases. Equilibrium is reached when the number of reptons promoted to saltation just balances the small absorption of grains in collisions. Since the process involves two species and thus two lengthscales  $l_{eje}$  and  $l_{drag}$ , the saturation length  $l_{sat}$  should be the largest of two. It should also be larger than the saltation length  $l_{sal}$ . For typical values of the shear velocity, the promotion of reptons to saltions is the limiting mechanism so that  $l_{sat}$  is given by the inertial length  $l_{drag}$ .

It is interesting to note that there has been only one previous derivation of the saturation length [45] which uses a completely different argument. Owen's criterion, predicts that the air-borne shear stress should have decreased to its threshold value at equilibrium. Simultaneously, the mean replacement rate  $\eta$  should vanish. On this basis, Sauermann *et al.* [45] proposed the empirical scaling law  $\eta \propto (u_*/u_{flu})^2 - 1$ , which, once reinjected in equation (27), leads to a saturation length  $l_{sat} \simeq \xi \rho_{sand}/\rho_{air} d$ , as found here.

Except the logarithmic dependence hidden in  $\xi$  the saturation length is independent of the shear velocity  $u_*$ . It scales as the grain size weighted by the sand to air density ratio and it is of the order of 10 m (table 1), as found experimentally [1].

### 3.4 Coupling between wind and shape

#### 3.4.1 Erosion rate, minimum size and barchan speed

In the previous section, we have seen how a sand bed is eroded by the wind. Now, where does the erosion takes place on a barchan and at which rate? To answer this question, let us introduce the local height  $h(x, y, t)$  of the dune and the volumic sand flux  $\mathbf{q}(x, y, t)$ . The conservation of matter reads:

$$\partial_t h + \nabla \cdot \mathbf{q} = 0 \quad (30)$$

If locally the sand flux is larger than the saturated flux then the sand flux decreases spatially and sand is deposited. If on the contrary the local sand flux is smaller than the saturated flux, the sand flux increases spatially and the sand bed is eroded.



**Fig. 17.** A sand patch (dome) on Tarfaya beach (southern Morocco) upwind the barchan field. The precursors to barchans directly appear with a length and a width of the order of 10 m.

What appends if a dune is smaller than the saturation length  $l_{sat}$ ? Because it is not saturated, the flux will increase continuously over the whole length of the dune. The dune will thus be eroded everywhere and will disappear. This explains very simply the experimental observation reported here (figures 6 and 7) that a small sandpile blown by the wind disappears. The order of magnitude of  $l_{sat}$  is also the length (and the width) with which the sand patches which will give barchans nucleate (figure 17). The introduction of the saturation length is thus very important because it explains the existence of the minimum length of the dune. We will see in the subsection devoted

to the wind around the dune that no other lengthscale appears in the problem so that it could be *the* relevant lengthscale in the problem.

To get a better view of the way a barchan is eroded, we can assume that it propagates with a constant shape and speed. Then  $h$  and  $q$  depend only on the variables  $x - ct$  and  $y$  so that the erosion rate  $\partial_t h$  is equal to  $-c\partial_x h$ . It means that the dune is eroded in the places where the slope along the wind direction is positive and the sand is deposited when this slope is on the contrary positive. When the brink and the crest coincide (for instance the large dune on figure 10), the horns and the slip face are the only places where the sand accumulates. For a dune presenting a small slip face (as the small dune on figure 10) there is a third region of accretion around the brink.

Let us consider a two-dimensional dune, invariant along the transverse direction  $y$  direction. Under the hypothesis of constant shape and speed, the conservation of matter (30) becomes  $\partial_x(q_x - ch) = 0$  which immediately integrates into:

$$q(x) = q_0 + ch(x) \quad (31)$$

where  $q_0$  is the sand supply i.e. the sand flux on the firm soil behind the dune. If the dune is sufficiently long, the sand flux  $q(x)$  is saturated at the crest of the dune. Then the propagation speed immediately derives from the equation (31):

$$c \simeq \frac{q_{sat} - q_0}{H} \quad (32)$$

Now, the three dimensional problem reduces to two dimensions if the conservation of matter (30) is integrated along the transverse direction  $y$ . Equation (31) thus holds if  $q$  and  $h$  are replaced by their average across the dune width. We make the reasonable assumption that the average height along a cross section of the dune scales on the overall height  $H$ . Then, the barchan speed  $c$  scales as  $(q_{sat} - q_0)/H$  provided that the flux be saturated at the crest. This  $1/H$  scaling of the speed was initially proposed by Bagnolds [1]. For typical values of the shear velocity (table 1),  $q_{sat}$  is of the order of a few hundred  $m^2/year$  which is the order of magnitude found for  $Q$  on the field (see section 2.3 and in particular equation (1)). Regarding the sand supply dependence, there has been no estimate of  $q_0$  so far. Field measurements show that Bagnolds scaling for the speed is imperfectly verified, a better approximation being  $c \simeq Q/(H_0 + H)$ . The existence of the cut-off scale  $H_0$  could come from the fact that the flux at the crest is not totally saturated but depends on the ratio of the dune length  $L$  to the saturation length  $l_{sat}$ .

#### 3.4.2 The wind shape relationship

By the erosion/accretion process, the wind modifies the topography. But in turn the topography modifies the wind. The wind velocity has been measured on the field around barchans of heights ranging from 2.5 m to 34 m (figure 19). It turns out that it is almost independent of this height. Even if the vertical variation of the velocity is not perfectly logarithmic [47], the shear velocity can be

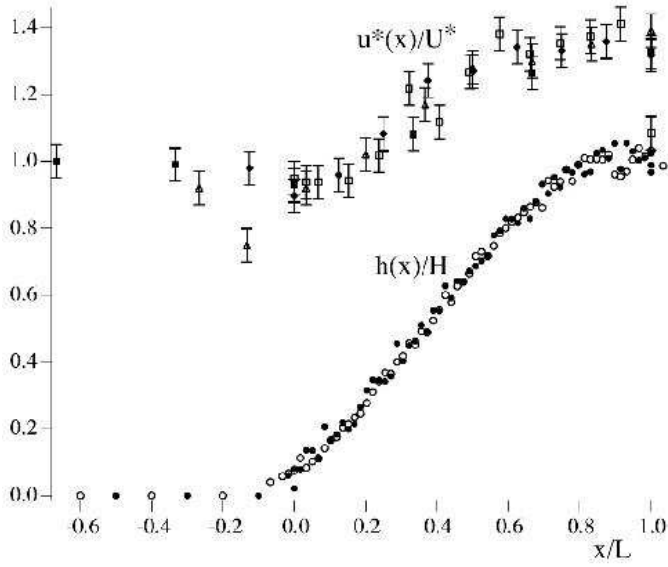


**Fig. 18.** The white and black circles are measurements of the central profile of a barchan ( $H = 2.5$  m and  $L = 36$  m) in the Negrita beach (south Morocco). The position  $x$  is rescaled by the dune length  $L$  and the profile  $h(x)$  by the dune height  $H$ . The shear velocity  $u_*$  on this dune is shown by white squares, rescaled by the shear velocity  $U_*$  far from the dune. Three others shear velocity profiles are shown, corresponding to barchans of various heights: the black squares ( $H = 34$  m and  $L = 200$  m) have been measured by Sauermann *et al.* [46] in Jericoacoara (Brazil), the white triangles ( $H = 10$  m and  $L = 100$  m) by Wiggs [20] in the Sultanate of Oman, and the black diamonds ( $H = 5.5$  m and  $L = 60$  m) by Howard *et al.* [8].

computed at different place on the dune. At the edge of the dune,  $u_*$  is observed to be slightly smaller than its value  $U_*$  far from the dune ( $u_*/U_* \simeq 0.9$ ). It then increases along the dune back: at the inflexion point,  $u_*/U_*$  is around 1.2 and it reaches 1.3 to 1.4 at the top of the dune.

The main theoretical problem is thus to determine the flow around a given sand bump and in particular the lee recirculations. The scaling laws of the wind velocity field are somehow simpler to determine than its spatial variations. For a fully turbulent flow, the Reynolds number  $u_*H/\nu$  based on the dune size, is typically of the order of  $10^6$ , and therefore viscous effects are negligible in front of inertial effects. This means that the whole velocity field is proportional to the shear velocity far from the dune, noted  $U_*$ .

Let us first consider the – theoretical – case of a vertically uniform turbulent flow. An homogeneous turbulent flow does not have any proper lengthscale. The whole flow is thus scale invariant: two dunes of the same shape but of different sizes should be surrounded by the same velocity field (in rescaled coordinates). To say it in crude way, if the dune size is multiplied by two, the velocity at the top remains the same (figure 19).

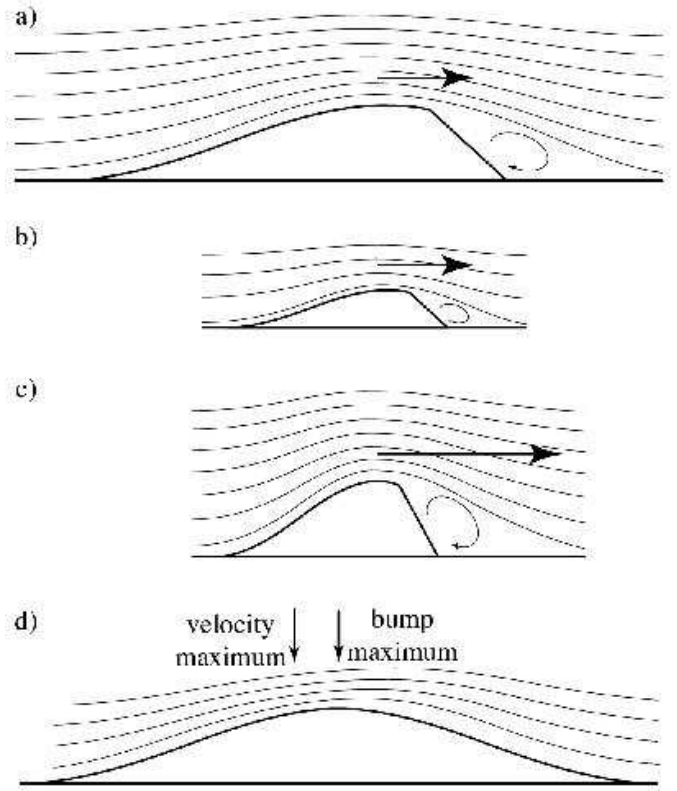


**Fig. 19.** A uniform ideal turbulent flow does not have any lengthscale, meaning that the velocity at the top of a bump (a) is the same if the bump is twice smaller (b). (c) Due to a pressure effect, the velocity at the top is larger if the bump length is divided by two but not the height. Even if the bump presents a symmetry downwind/upwind (d), the velocity field does not present the same symmetry: the velocity is larger before the crest than after so that the velocity maximum is displaced upwind with respect to the bump maximum.

The main effect is related to changes of pressure [48, 49], which is a non local function of the shape. In other words, the pressure and thus the velocity at some point of the dune is a function of the whole dune shape. Denoting by  $h(x)$  the local height of a two-dimensional dune (as that shown on figure 19), we can conclude from the previous considerations that the shear velocity  $u_*$  depends only on the slope  $\partial_x h$ , which is the only dimensionless field describing the dune shape. But it is a non local function of  $\partial_x h$ . Consider the dune shown in figure 19 (a) and shrink it horizontally by a factor of two (figure 19 c), the wind will be larger. This means that the velocity is sensitive to the aspect ratio of the bump, to a kind curvature rescaled by the size of the dune. This pressure effect is a linear effect and exists even in the limit of small bumps.

If the direction of the wind is a symmetry axis for the dune, the wind is symmetrical as well. But if the dune admits a symmetry axis perpendicular to the wind (figure 19 d), this symmetry upstream/downstream is broken by the velocity field, as in the classical case of the flow around a sphere. This corresponds to an irreversible feature of

the flow: the streamlines are different when the flow is reversed. This asymmetry upwind/downwind is a non-linear effect of the streamlines curvature on turbulence [49]. It is an inertial effect which, as previously, is scale invariant.

If the backward face is steep, the flow can no longer follow the form of the dune. The boundary layer separates from the bed and reattaches down wind, enclosing a separation bubble. Inside this bubble, the wind flows back toward the obstacle so that the velocity profile is no longer logarithmic. Note that even the exact conditions under which flow separates are not clear yet. The best idea to model flow separation has been proposed by Zeman and Jensen [50]. They suggested that the flow outside the recirculation bubble was precisely that would have been observed if the streamlines separating the recirculating flow from the turbulent boundary layer were solid. Again, this idea of a dune envelope seems correct to the first order but should be corrected by two effects. First, it is somehow arbitrary to prolong the dune by a surface of same roughness. Second, the separation surface is well defined on the average but fluctuates in time while the actual sand bed does not.

To summarise, the velocity field is scale invariant in the ideal case of a vertically uniform turbulent flow. The velocity increases in regions where the curvature is negative. In the case of a symmetric bump, the velocity field around this bump does not present the same symmetry: the velocity is larger before the crest than after so that the velocity maximum is displaced upwind with respect to the bump maximum (figure 19 d). This means that the velocity is also sensitive to the local slope.

All these properties are present in the expression given by Jackson and Hunt [51,52,53] and simplified by Kroy *et al.* [19] for the flow around a smooth flat hill. In two dimensions, it reads:

$$u_*^2(x) = U_*^2 \left( 1 + A \int \frac{ds}{\pi s} \partial_x h(x-s) + B \partial_x h(x) \right) \quad (33)$$

where  $A$  and  $B$  are almost constant (see below). Jackson and Hunt [51] have predicted the values of  $A$  and  $B$  in the limit of a vanishing aspect ratio  $H/L$  – at least smaller than 0.05 but equation 33 can also be used for dunes, introducing effective coefficients  $A$  and  $B$ . The whole field  $u_*(x)$  is proportional to  $U_*$  which is the velocity above a flat bed ( $\partial_x h = 0$ ). It does not depend on the overall bump size since it is a – non local – function of the slope, only. It is modulated by the local slope (the  $B$  term) and by a ‘dimensionless curvature’ (the  $A$  term) which takes the form of a convolution of the slope by the kernel  $1/x$ . Equation (33), used on a dune prolonged by the separation bubble modelled empirically, is the best known analytical model of wind above a barchan. It has for instance been used by Weng *et al.* [53] who computed the erosion rate of a barchan and by Kroy *et al.* [19] who integrated numerically a complete model of dunes.

In the case of a turbulent boundary layer, there is actually a characteristic lengthscale, the soil roughness  $z_0$ , which breaks the scale invariance. The previous effects remains valid but the fact that the velocity profile depends

logarithmically on height leads to logarithmic corrections in the dune length to roughness ratio [51,48,52,53,49]. For instance, in the original Jackson and Hunt model, the asymmetry upwind/downwind was directly related to the soil roughness ( $B \propto 1/\ln(L/z_0)$ ). We see on this example that the effect of the roughness  $z_0$  is not negligible:  $\ln(L/z_0)$  is of the order of 10 for dunes. But it also shows that it is almost independent of the dune size: a factor 10 on  $L$  leads to a variation of 20% of  $\ln(L/z_0)$ . As a conclusion, the wind scale invariance is a very good approximation, even with roughness effects. This analysis is confirmed by the wind measurements presented on figure 18.

### 3.5 Avalanches

The last important phenomenon takes place at the slip face. If the sand flux is not saturated upwind the dune, the back of the dune is eroded and the sand flux increases. This sand is deposited soon after the brink, on the slip face, and forms a kind of snowdrift. As shown on figure 20 when the slope becomes locally larger than the static friction coefficient  $\mu_s$ , an avalanche spontaneously nucleates which propagates downward the slip face. It is a dense flow in which grains always remain in contact and which is limited to a thin layer at the surface of the slip face. As in solid friction [54], this flow stops roughly when the slope as decreased below the dynamical friction coefficient  $\mu_d$ . The modelling of avalanches have recently received pretty high attention from the physicists [55,56,57]. In particular, we now have accurate descriptions of granular surface flows by Saint-Venant equations [57,58,59] governing the evolution of the free surface, the flowing height and the mean velocity.

Fortunately, we do not need such refined models to understand avalanches in the case of dunes. Note first that the avalanche duration (a few seconds to one minute) is always smaller than the time separating avalanches (a few minutes to a few days) which is much smaller than the turnover time. Note also that the details of the slip face do not react on the dune back since it is inside the separation bubble. Each individual avalanche propagates downward the steepest slope and stops when the slope has decreased below  $\mu_d$ . Thus, avalanches may be considered as an instantaneous slope relaxation process which displaces sand along the steepest slope, when the later is larger than  $\mu_d$ .

## 4 Conclusion: open problems

### 4.1 Field observations

In the first part of this article, we have presented the field observations about barchan dunes. Let us give here a short summary. A barchan is a crescentic dune propagating downwind on a firm soil. When the direction of the wind is almost constant, these dunes can maintain a nearly constant shape and size for very long times. The barchan mean velocity  $c$  scales approximately with the inverse of



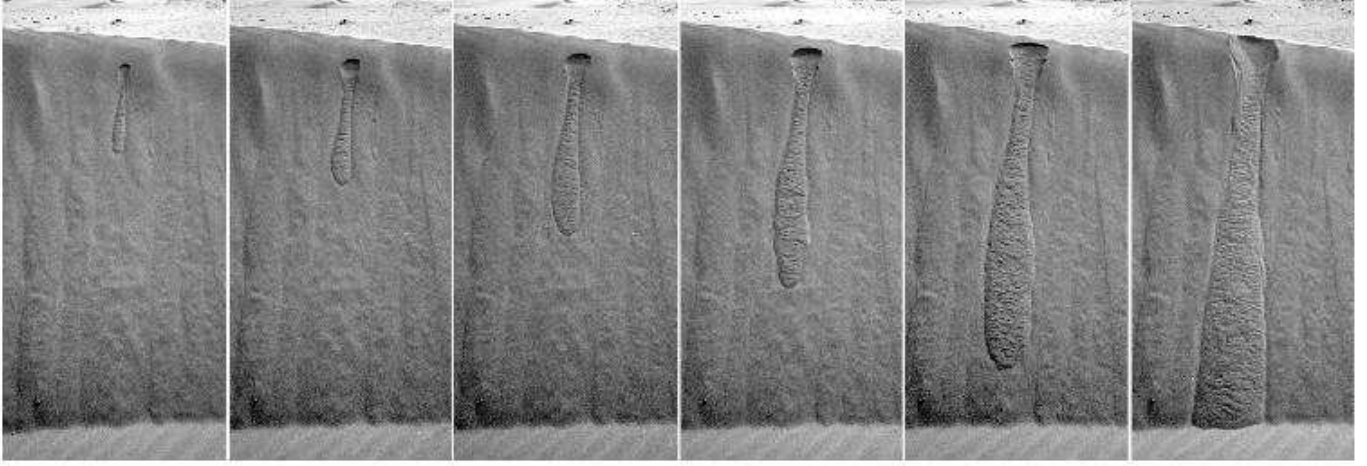


**Fig. 20.** When an avalanche spontaneously nucleates, usually in the middle of the deposition zone, it both propagates downhill and uphill and stops when the local slope has decreased below the dynamical angle.

its height  $H$ :  $c \simeq Q/(H_0 + H)$ . It turns out that the flux  $Q$  (typically  $100 \text{ m}^2/\text{s}$ ) and the height cut-off  $H_0$  (of the order of  $1 \text{ m}$ ) depend on time (probably through meteorological variations) and on the dune field. The barchan height  $H$ , its length  $L$ , its width  $W$  and the length of its horns  $L_{\text{wings}}$  are, on the average, related one to the others by linear relationships which depend on the dune field but apparently not on the wind variations. The typical proportions of large dunes are 9 for the ratio width to height, 6 for the ratio length to height and 9 for the ratio horn length to height. However,  $H$ ,  $L$  and  $W$  are not proportional. It means that barchans are not scale invariant. The existence of a characteristic size is confirmed by the fact that no barchan lower than  $1 \text{ m}$  are observed.

The first thing to note is the strong dispersion of field measurements: typically 50 dunes have to be measured to establish correctly one relation. As a consequence, there is few reliable data despite the numerous studies. Moreover, the barchans morphology and speed obviously depend on local parameters which have not been identified so far: no systematic study has been made on the influence of the wind speed, its fluctuations in direction, the nature of the soil, the sand supply, the vicinity of other dunes, etc. One of the goal, in the future, will be the establishment of universal relationships integrating the dependence on local parameters. The existence of a minimum size of dune also rises questions. What determines this size? If a small conical sandpile quickly disappears when eroded by the wind, how can barchan form?

These questions concern barchans in their individual behaviour. Another class of problems concerns the global dynamics of dune fields (ergs [60,61]). What determines the mean spacing between dunes? What selects the size of the dune? What determines the sand supply at the back of the dune and the leak by the horns? Is sand transport more efficient, on the average, in a barchan field when compared to saltation over the desert floor? What are the precise conditions under which linear transverse dunes appear instead of a barchan field? These questions have re-

ceived pretty low attention. For instance there has been one measurement of crescent dune spacing in Namibia by Lancaster [62] who have found a linear relation between spacing and height. But it was in a field in which the dunes are very close one to the others. Another example is provided by Hastenrath [6,9], who have computed the histogram of dune heights in the Pampa de La Joya (southern Peru). In 1964 it exhibits a sharp peak around  $3.5 \text{ m}$  and in 1983 around  $1.5 \text{ m}$ . These measurements show that the dune fields are homogeneous in dune heights but are not sufficient to determine the origin of the height selection. Concerning the average sand flux, the bulk transport i.e. the transport of sand by the dunes have been measured by Lettau and Lettau [63] also in the Pampa de La Joya. The total flux between 1958 and 1964 was around  $1 \text{ m}^2/\text{year}$  which is a hundred times smaller than the saturated flux on a flat soil: bulk transport is apparently much less efficient than saltation over the flat soil. If the wind is able to transport much more sand in saltation, why does the flux saturates in the places where barchans form? How and where can a dune field form? Moreover they have shown that the mean flux increases downwind meaning that the soil is eroded (at a rate  $200 \mu\text{m}/\text{year}$ ). This article is the only tentative of description of sand fluxes at the scale of the dune field.

As a conclusion, further studies will have to focus on the detailed characterisation of barchan fields, aiming to get sufficient statistics, as for the Pampa de La Joya.

## 4.2 Dynamical mechanisms and dune modelling

In the present state of the art, most of the dynamical mechanisms important for barchans formation and propagation have been identified. The explanation of dune propagation is simple: the back of the dune is eroded by the wind and the sand transported in the air is deposited at the brink and is redistributed on the slip-face by avalanches. The detailed description can be decomposed into two parts: the sand transport over a sand bed for a

given wind speed on the one hand and the wind speed around a given bump on the other hand.

In this paper, we have proposed a coherent picture of sand transport. If the wind strength is sufficiently large, grains can be directly entrained by the wind. They roll on the soil, take-off, fall back again, rebound, are accelerated by the wind, fall back again and so on. Once the transport initiated, another mechanism of production takes over the direct aerodynamic entrainment. When the grains in saltation collides the sand bed, they splash up a number of low energy reptons which are accelerated by the wind and become saltons. So, in a first stage, the sand flux increases exponentially. To accelerate the grains, the wind has to give them some of its momentum. Its strength therefore decreases as the sand flux increases. The transport reaches equilibrium when the shear velocity has so decreased that the number of reptons promoted to saltation just balance the number of saltons remaining trapped after collisions with the sand bed. This saturation process takes time – and space – to establish. The space lag between the edge of a sand sheet blown by the wind and the point at which the flux saturates is given by the inertial length  $l_{drag}$  defined as the distance needed for a repton to become a salton i.e. to be accelerated to the wind velocity. This saturation length is the only relevant lengthscale of the problem and is directly related to the minimum length of barchans.

There are still a few points concerning sand transport which need to be clarified. A first important aim is to re-examine experimentally the difference between saltation and reptation, in particular the controversial scaling of the saltation height and length, the influence of a lateral or longitudinal slope, etc. A second problem is the anomalous scaling of the saturated flux, the apparent roughness and probably other quantities, with the grain diameter. This suggests the existence of unknown mechanisms which would be worth studying. A third interesting study would be to reexamine experimentally the saturation process, in particular the mechanisms and the scaling of the saturation length.

The problem of the turbulent wind flow over a dune is different. On the one hand, there exist well known methods to solve this problem numerically even though they take a lot of computation time. On the other hand, we know the basic principles: the velocity field is scale invariant and is proportional to the wind velocity far from the obstacle; it increases on a bump and is larger for an upwind than for a downwind slope. In middle, very few models have been proposed which are both realistic and sufficiently simple to be understood. The most useful is certainly that of Jackson and Hunt [51]. The main open problem is the description of the recirculation bubble which requires either a full 3D simulation or very crude empirical assumptions.

Theoretical and numerical studies of dunes are particularly interesting and helpful to understand their dynamics. The first aim to compute numerically the rate at which sand is eroded or deposited on barchan dunes goes back to Howard *et al.* [8]. To do so, they used the topography of an actual barchan together with laboratory measure-

ments of the velocity field around a scale model of this dune. This work was completed by Weng *et al.* [53] who also computed the erosion rate but this time, using Jackson and Hunt approximation. Wipperman and Gross [13] used a simpler model of flow over hills but computed the evolution in time of a sandpile. They were able to get a crescentic dune propagating at a nearly constant velocity. However, due to the complexity of their model, this computation could only be performed on one turnover time. More recently, numerical models of the transient of formation of two dimensional dunes were proposed by Stam [16] and van Dijk *et al.* [18]. Finally, Kroy *et al.* [19] have proposed a complete model which takes into account all the known mechanisms and which also leads to reasonable barchan dunes. In part 2, we will simplify this model and investigate theoretically the shape and velocity of dunes. Much simpler numerical models such as cellular automata [14,15,17] have been proposed in the last decade which do not lead to realistic isolated dunes but which are able to describe patterns of interacting dunes and to test the influence of variable winds. The next step is now to use numerical simulations or laboratory experiments to supply for the lack of control in field studies. They will certainly help to find the important parameters for the selection of dunes shape, size and velocity but also to look at the interaction between dunes and even to test the influence of complex wind regimes.

## Acknowledgments

B. Andreotti and S. Douady would like to thank F. Naim, M. Naim for their welcome and for the use of the Cemagref wind tunnel. The authors wish to thank P. Hersen and Y. Couder for critical reading of the manuscript. This work benefited from the ‘Action Concertée Incitative’ of the french ministry of research.

## References

1. R.A. Bagnold, *The physics of blown sand and desert dunes*, Chapman and Hall, London (1941).
2. H.J.L. Beadnell, The sand-dunes of the Libyan desert, *Geographical Journal* **35**, 379-395 (1910).
3. H.J. Finkel, The barchans of southern Peru, *Journal of Geology* **67**, 614-647 (1959).
4. A. Coursin, *Bulletin de l'IFAN* **3**, 989-1022 (1964).
5. J.T. Long and R.P. Sharp, Barchan dune movement in imperial valley, California, *Geological Society of America*, **75**, 149-156 (1964).
6. S.L. Hastenrath, The barchans of the Arequipa Region, Southern Peru, *Zeitschrift für Geomorphologie* **11**, 300-331 (1967).
7. R.M. Norris, Barchan dune of imperial valley, California, *J. Geol.* **74**, 292-306, (1966).
8. A.D. Howard, J.B. Morton, M. Gad el Hak and D.B. Pierce, Sand transport model of barchan dune equilibrium, *Sedimentology* **25**, 307-338 (1978).
9. S.L. Hastenrath, The barchans of Southern Peru revisited, *Zeitschrift für Geomorphologie* **31-2**, 167-178 (1987).

10. M.C. Slattery, Barchan migration on the Kuiseb river delta, Namibia, *South African Geographical Journal* **72**, 5-10 (1990).
11. P.A. Hesp and K. Hastings, Width, height and slope relationships and aerodynamic maintenance of barchans, *Geomorphology* **22**, 193-204, (1998).
12. G. Sauermann, P. Rognon, A. Poliakov and H.J. Herrmann, The shape of barchan dunes of southern Morocco, *Geomorphology* **36**, 47-62 (2000).
13. F.K. Wippermann and G. Gross, The wind-induced shaping and migration of an isolated dune: numerical experiment, *Boundary-Layer Meteorology* **36**, 319-334 (1986).
14. H. Nishimori and N. Ouchi, Formation of ripples patterns and dunes by wind blown sand, *Phys. Rev. Lett.* **71**, 197-200 (1993).
15. B.T. Werner, Aeolian dunes: computer simulations and attractor interpretation, *Geology* **23**, 1107-1110 (1995).
16. J.M.T. Stam, On the modelling of two-dimensional aeolian dunes, *Sedimentology* **44**, 127-141 (1997).
17. H. Nishimori and M. Yamasaki, A minimal model approach for the morphodynamics of dunes, in *Physics of dry granular media*, Hermann, Hovi and Luding eds. Kluwer, Dordrecht, 347-352 (1998).
18. P.M. van Dijk, S.M. Arens, J.H. van Boxel, Aeolian processes across transverse dunes. II: modelling the sediment transport and profile development, *Earth Surface Processes and Landforms* **24**, 319-333 (1999).
19. K. Kroy, G. Sauermann and H.J. Herrmann, a minimal model for sand dunes, submitted to *Phys. Rev. Lett.*, cond-mat/0101380 (2001).
20. R. Cooke, A. Warren and A. Goudie, *Desert geomorphology*, UCL Press, London (1993).
21. O. Dauchot, F. Lechenault and C. Gasquet, *Barchan dunes in the lab*, cond-mat/0108378.
22. S.P. Gay, Observations regarding the movement of barchan sand dunes in the Nazca to Tanaca area of southern Peru, *Geomorphology* **27**, 279-293 (1999).
23. J.R.L. Allen, *Current ripples: their relation to patterns of water and sediment motion*. Amsterdam: Elsevier/North Holland (1968).
24. T. Oulehri, Etude géodynamique des migrations de sables éoliens dans la région de Laayoune (Nord du Sahara marocain), PhD thesis, Université Paris 6, France.
25. P. Nalpanis, J.C.R. Hunt and C.F. Barrett, Saltating particles over flat beds, *J. Fluid Mech.* **251**, 661-685 (1993).
26. M. Sørensen, Estimation of some aeolian saltation transport parameters from transport rate profiles, in *International workshop on the physics of blown sand*, Barndorff-Nielsen, Moller, Rasmussen and Willets eds. University of Aarhus, 141-190 (1985).
27. J.L. Jensen and M. Sorensen, Estimation of some aeolian saltation transport parameters: a re-analysis of Williams data, *Sedimentology* **33**, 547-558 (1986).
28. P.R. Owen, Saltation of uniform grains in air, *J. Fluid. Mech.* **20**, 225-242 (1964).
29. M. Sørensen, An analytic model of wind-blown sand transport, *Acta Mechanica [Suppl]* **1**, 67-81 (1991).
30. L. Quartier, B. Andreotti, A. Daerr and S. Douady, Dynamics of a grain on a sandpile model, *Phys. Rev E* **62**, 8299-8307 (2000).
31. R.S. Anderson and P.K. Haff, Simulation of aeolian saltation, *Science* **241**, 820-823 (1988).
32. R.S. Anderson and P.K. Haff, Wind modification and bed response during saltation of sand in air, *Acta Mechanica [Suppl]* **1**, 21-51 (1991).
33. F. Rioual, A. Valance and D. Bideau, Experimental study of the collision process of a grain on a two-dimensional granular bed, *Phys. Rev. E* **62**, 2450-2459 (2000).
34. R.S. Anderson, M. Sørensen and B.B. Willets, A review of recent progress in our understanding of aeolian sediment transport, *Acta Mechanica [Suppl]* **1**, 1-19 (1991).
35. K. Lettau and H.H. Lettau, in *Exploring the world's driest climate*, Lettau and Lettau eds., Madison, Wisconsin (1978).
36. B.R. White and H. Mounla, An experimental study of Froude number effect on wind-tunnel saltation, *Acta Mechanica [Suppl]* **1**, 145-157 (1991).
37. K.R. Rasmussen, H.E. Mikkelsen, Wind tunnel observations of aeolian transport rates, *Acta Mechanica [Suppl]* **1**, 135-144 (1991).
38. K.R. Rasmussen and J.D. Iversen, Grain dynamics and wind-flow in a variable slope wind tunnel, in *Sustainable development in arid zones*, edited by S.A.S. Omar, R. Misak, D. Al-Ajmi and N. Al-Awadhi, Balkema, Rotterdam, The Netherland (1996).
39. K.R. Rasmussen, J.D. Iversen and P. Rautahaimo, Saltation and wind flow interaction in a variable slope wind tunnel, *Geomorphology* **17**, 19-28 (1996).
40. A.D. Howard, Effect of slope on the threshold of motion and its application to orientation of wind ripples, *Bulletin Geological Society of America* **88**, 853-856 (1977).
41. J. Hardisty and J.R.S. Whitehouse, Evidence for a new sand transport process from experiments on Saharan dunes, *Nature* **332**, 532-534 (1988).
42. J.D. Iversen and K.R. Rasmussen, The effect of surface slope on saltation threshold, *Sedimentology* **41**, 721-728 (1994).
43. M.R. Raupach, Saltation layers, vegetation canopies and roughness lengths, *Acta Mechanica [Suppl]* **1**, 83-96 (1991).
44. B.B. Willets, J.K. McEwan and M.A. Rice, Initiation of motion of quartz sand grains, *Acta Mechanica [Suppl]* **1**, 123-134 (1991).
45. G. Sauermann, K. Kroy and H.J. Herrmann, A continuum saltation model for sand dunes, *Phys. Rev. E* **64**, 031305 (2001).
46. Sauermann G., PhD Thesis, Stuttgart University, edited by Logos Verlag (Berlin) (2001).
47. K.R. Mulligan, Velocity profiles measured on the windward slope of a transverse dune, *Earth surface processes and Landforms* **13**, 573-582 (1988).
48. O. Zeman and N-O. Jensen, Modification of turbulence characteristics in flow over hills, *Quart. J. R. Met. Soc.* **113**, 55-80 (1987).
49. J.H. van Boxel, S.M. Arens, P.M. van Dijk, Aeolian processes across transverse dunes. I: Modelling the air flow, *Earth Surface Processes and Landforms* **24**, 255-270 (1999).
50. N-O. Jensen and O. Zeman, in *International workshop on the physics of blown sand*, Barndorff-Nielsen, Moller, Rasmussen and Willets eds. University of Aarhus, 351-368 (1985).
51. P.S. Jackson and J.C.R. Hunt, Turbulent wind flow over a low hill, *Quart. J. R. Met. Soc.* **101**, 929-955 (1975).
52. J.C.R. Hunt, S. Leibovitch and K.J. Richards, Turbulent shear flows over low hills, *Quart. J. R. Met. Soc.* **114**, 1435-1470 (1988).

53. W.S. Weng, J.C.R. Hunt, D.J. Carruthers, A. Warren, G.F.S. Wiggs, I. Livingstone and I. Castro, Air flow and sand transport over sand-dunes, *Acta Mechanica* [Suppl] **2**, 1-22 (1991).
54. C. Coulomb, *Mémoires de Mathématiques et de Physique Présentés l'Académie Royale des Sciences par Divers Savants et Lus dans les Assemblées*, 343 (Imprimerie Royale, Paris, 1773)
55. J.P. Bouchaud, M. Cates, J.R. Prakash and S.F. Edwards, A model for the dynamics of sandpile surfaces, *J. Phys. France I* **4**, 1383-1410 (1994).
56. T. Boutreux, E. Raphael and P.G. de Gennes, Surface flows of granular material: a modified picture for thick avalanches, *Phys. Rev. E* **58**, 4692-4700 (1998).
57. O. Pouliquen, On the shape of granular fronts down rough inclined planes, *Phys. Fluids* **11**, 1956-1958 (1999).
58. S. Douady, B. Andreotti and A. Daerr, On granular surface flow equations, *Eur. Phys. J. B* **11**, 131-142 (1999).
59. B. Andreotti and S. Douady, Selection of velocity profile and flowing depth in granular flows, *Phys. Rev. E* **63**, 1305-1312 (2001).
60. I.G. Wilson, Aeolian bedforms, their development and origin, *Sedimentology* **19**, 173-210 (1972).
61. I.G. Wilson, Ergs, *Sedimentary Geology* **10**, 77-106.
62. N. Lancaster, Dunes on the skeleton coast, Namibia (South West Africa): geomorphology and grain size relationships, *Earth surface processes and Landforms* **7**, 575-587 (1982).
63. K. Lettau and H.H. Lettau, Bulk transport of sand by the barchans of La Pampa La Hoja in southern Peru, *Zeitschrift für Geomorphologie* **13**, 182-195 (1969).